https://doi.org/10.5194/bg-2019-484
Preprint. Discussion started: 21 January 2020
© Author(s) 2020. CC BY 4.0 License.

Biogeosciences
Discussions

Dynamics of environmental conditions during a decline of a *Cymodocea nodosa* meadow

Mirjana Najdek[1], Marino Korlević[1], Paolo Paliaga[2], Marsej Markovski[1], Ingrid Ivančić[1], Ljiljana Iveša[1], Igor Felja[3] and Gerhard J. Herndl[4,5]

[1]Center for Marine Research, Ruđer Bošković Institute, G. Paliaga 5, 52210 Rovinj, Croatia

[2]Department of Natural and Health Sciences, University of Pula, Zagrebačka 30, 52100 Pula, Croatia

[3]Department of Geology, Faculty of Science, University of Zagreb, Horvatovac 102a, 10000 Zagreb, Croatia

[4]Limnology and Bio-Oceanography, Center of Functional Ecology, University of Vienna, Althanstrasse 14, 1090 Vienna, Austria

[5]NIOZ, Department of Marine Microbiology and Biogeochemistry, Royal Netherlands Institute for Sea Research, Utrecht University, PO Box 59, Alberta, Den Burg, 1790, The Netherlands

Correspondence to: Mirjana Najdek (najdek@cim.irb.hr)

https://doi.org/10.5194/bg-2019-484
Preprint. Discussion started: 21 January 2020
© Author(s) 2020. CC BY 4.0 License.

Biogeosciences Discussions

Abstract. The dynamics of the physicochemical and biological parameters were followed during the decline of a *Cymodocea nodosa* meadow in the northern Adriatic Sea from July 2017 to October 2018. During the regular growth of *C. nodosa* from July 2017 to March 2018, *C. nodosa* successfully adapted to the changes of environmental conditions and prevented H_2S accumulation by its re-oxidation, supplying the sediment with O_2 from the water column and/or leaf photosynthesis. The *C. nodosa* decline was most likely triggered in April 2018 by a reduction of light availability which affected photosynthesis of *C. nodosa* and the oxidation capability of below-ground tissue. Simultaneously, a depletion of oxygen due to intense oxidation of H_2S occurred in the sediment, thus creating anoxic conditions in most of the rooted areas. These linked negative effects on the plant performance caused an accumulation of H_2S in the sediments of the *C. nodosa* meadow. During the decay of above- and below-ground tissues, culminating in August 2018, high concentrations of H_2S were reached and accumulated in the sediment as well as in bottom waters. The influx of oxygenated waters in September 2018 led to the re-establishment of H_2S oxidation and recovery of the below-ground tissue. Our results indicate that if disturbance of environmental conditions, particularly those compromising the light availability, takes place during the recruitment phase of plant growth when metabolic needs are at maximum and stored reserves minimal, a sudden and drastic decline of the seagrass meadow occurs.

https://doi.org/10.5194/bg-2019-484
Preprint. Discussion started: 21 January 2020
© Author(s) 2020. CC BY 4.0 License.

1 Introduction

Seagrasses are important ecosystem engineers constructing valuable coastal habitats which play a key role in the preservation of marine biodiversity and carbon sequestration (Duarte et al., 2005). Seagrasses extend their active metabolic surfaces (i.e., leaves, rhizomes and roots) into the water column and in the sediment, where root activity might modify the chemical conditions (Marbà and Duarte, 2001). Their canopies and dense meadows are responsible for trapping substantial amounts of sediment particles and organic matter enhancing water transparency and sediment stability with the dense network formed by the rhizome (Gacia and Duarte, 2001; Hendriks et al., 2008; Widdows et al., 2008). Seagrass rhizospheres store organic matter (Pedersen et al., 1997), promote sulfate reduction (Holmer and Nielsen, 1997), release oxygen (Pedersen et al., 1998) and alter sediment redox potential.

Seagrasses require some of the highest levels of solar radiation of any plant worldwide to provide oxygen to roots and rhizomes and support a large amount of non-photosynthetic tissue (Orth et al., 2006). These high solar radiation requirements make seagrasses sensitive to environmental changes, especially those that deteriorate light availability, such as sediment loading, eutrophication or epiphyte cover on seagrass leaves (Terrados et al., 1998; Halun et al., 2002; Brodersen et al., 2015; Costa et al., 2015). Seagrasses have adapted to a highly variable light environment providing tolerance to short-term periods of low light conditions by balancing carbon supply and respiratory requirements. In a healthy growing population this balance is achieved by increasing the photosynthetic activity, re-allocation of carbohydrate reserves from rhizomes and slowing down growth rates (Collier et al., 2009). Beside metabolic and physiological changes, stress responses under poor light conditions include shedding of leaves and shoots and production of new, altered tissue. At sub-lethal light levels, these changes may be permanent. Below these species-specific minimum light requirements seagrass populations are dying off (Collier et al., 2012). Membrane lipids, particularly polyunsaturated fatty acids (PUFA), as the most responsive constituents have a major role in the adaptation processes of primary producers to fluctuating environmental factors, such as temperature, irradiance or salinity (Viso et al., 1993; Lee et al., 2007; Schmid et al., 2014; Sousa et al., 2017; Beca-Carretero et al., 2018; Beca-Carretero et al., 2019). The changes in the unsaturation degree (UND) of membrane fatty acids affect the maintenance of membrane functions and its resistance to cold stress or poor light conditions. UND depends mostly on the variation of α-linolenic (C18:3n-3, ALA) and linoleic (C18:2n-6, LA), the major unsaturated fatty acids in leaves, implicated in the evolution of oxygen during photosynthesis.

LA and ALA are derived from oleic acid by desaturation in the chloroplast and this conversion considerably declines in the dark, being completely inhibited by anaerobiosis (Harris and James, 1965).

Sediments inhabited by seagrasses are usually anoxic, highly reduced and rich in sulfide (H_2S), a strong phytotoxin (Koch and Erskine, 2001) which has been implicated in several die-off events of seagrasses (Carlson et al., 1994; Borum et al., 2005; Krause-Jensen et al., 2011). H_2S is produced by sulfate-reducing bacteria that use sulfate as a terminal electron acceptor for the mineralization of organic matter (Jørgensen, 1977; Capone and Kiene, 1988, Canfield et al., 1993). High H_2S concentrations may occur as a consequence of enhanced mineralization due to increased temperature, organic loading or oxygen depletion (Moeslund et al., 1994; Pérez et al., 2007; Mascaró et al., 2009). Under these conditions, sulfides may intrude into plant. Re-oxidation of H_2S in the rhizosphere by incorporation of S^0 in the below-ground tissue has been recognized as a major survival strategy of seagrasses in sulfidic sediments (Pedersen et al., 2004; Holmer et al., 2005; Hasler-Sheetal and Holmer, 2015). Generally, the synergistic effect of oxygen depletion and other stresses, such as sulfide toxicity may shorter the survival of benthic communities and possibly accelerate mortality events (Vaquer-Sunyer and Duarte, 2010).

The seagrass *Cymodocea nodosa* (Ucria) Ascherson is a common species throughout the Mediterranean, adapted to a wide range of coastal habitats and environmental conditions (Terrados and Ros, 1992; Marbà et al., 1996; Pedersen et al., 1997; Zavodnik et al., 1998; Cancemi et al., 2002; Agostini et al., 2003). During this study, performed from July 2017 to October 2018 in Saline Bay (northern Adriatic Sea), a considerable decline of *C. nodosa* meadow occurred. We conducted a series of monthly physicochemical and biological measurements in *C. nodosa* tissues, sediment underlying the *C. nodosa* meadow, non-vegetated sediments and surrounding water to i) determine the link between ambient seawater and sediment environmental factors influencing the growth of *C. nodosa*, ii) document the response of *C. nodosa* to the changes in environmental conditions that led to the meadow decline and iii) evaluate the conditions leading to the decline of *C. nodosa*.

2 Materials and methods

2.1 Study site

Saline Bay is located 4 km northwest of Rovinj (Croatia) at the coast of the northern Adriatic Sea (45°7′5″N; 13°37′20″E). The bay represents the terminal shallow part of an 800 m long inlet, open towards the northwest. The southeastern coast of Saline Bay is characterized by

https://doi.org/10.5194/bg-2019-484
Preprint. Discussion started: 21 January 2020
© Author(s) 2020. CC BY 4.0 License.

relatively pristine conditions, while the northwestern littoral part has been completely modified by the excavation of coastal mud and the addition of large amounts of gravel to create an artificial beach. Large amounts of silty red soil (*terra rossa*) can be found in the south eastern inner part of the bay in a large muddy flatland which is slowly being eroded by the sea and rain weathering. The main input of freshwater to the bay represents land drainage canals since the year 2017. Even though Saline Bay is protected from the prevailing winds (from the NE and SE) circulations from the northwestern quadrant can occasionally trigger bigger waves resuspending the surface sediments and giving the waters a muddy appearance. A monthly field survey carried from July 2017 to October 2018 has revealed a substantial decline of *C. nodosa.* At the beginning of this study, the seafloor was covered with large meadows spreading from the southwestern coastal area (1.5 m depth) toward the central part of the bay (4 m depth), while at the end of the study only a few small patches persisted in tiny stripes along the shoreline.

2.2 Sampling

Seawater for analyses of nutrients, chlorophyll a (Chl *a*), particulate matter concentration and prokaryotic abundance was sampled using plastic containers (10 L). *C. nodosa* was collected together with rhizomes, roots and epiphytic macroalgae by divers using the quadrat sampling method. Three quadrats (20 x 20 cm) were randomly scattered in positions of maximum seagrass coverage (e.g. 100 %). Sediment samples were collected inside vegetated and non-vegetated sediment by divers using plastic core samplers (15 cm, 15.9 cm^2). For granulometric composition, organic matter, prokaryotic abundance, total lipids and fatty acid analyses, the cores were cut into 1 cm sections to a depth of 8 cm and lyophilized, except of sections for prokaryotic abundance analysis, that were weighted (approx. 2 g) and fixed with formaldehyde (final conc. 4% v/v) immediately after slicing the sediment core.

2.3 Temperature (T) and salinity (S) measurements

T was measured continuously (in 30 min. intervals) using HOBO pendant temp/light Data Loggers (Onset, USA) which were replaced at each sampling. S was measured on sampling dates by a pIONneer 65 probe (Radiometer analytical, Copenhagen).

2.4 Inorganic nutrients, Chl *a* and particulate matter (PM) analysis

Nitrate (NO_3), nitrite (NO_2), ammonia (NH_4), phosphate (PO_4) and silicate (SiO_4) were analyzed spectrophotometrically according to Strickland and Parsons (1972). Chl *a* was

https://doi.org/10.5194/bg-2019-484
Preprint. Discussion started: 21 January 2020
© Author(s) 2020. CC BY 4.0 License.

determined by the fluorometric procedure after filtration of seawater through Whatman GF/F filters and extraction in 90 % acetone (Holm-Hansen et al., 1965). PM was determined gravimetrically after filtering up to 5L seawater on pre-weighed, combusted Whatman GF/F filters which were dried (at 60°C) and reweighed.

2.5 Determining prokaryotic abundance

For determining the prokaryotic abundance in seawater, 2 ml of formaldehyde (final conc. 4% v/v) fixed samples were stained with 4,6-diamidino-2-phenylindol (DAPI, 1 μg mL^{-1} final conc.) for 10 min (Porter and Feig, 1980). In sediment samples, prokaryotes were detached from the sediment particles by addition of Tween 80 (0.05 mL) and ultrasonicated for 15 min (Epstein and Rossel 1995). After sonication, 1 mL of the supernatant was stained with DAPI (final conc. 5 μg/mL). DAPI stained samples were filtered onto black polycarbonate filters (Whatman, Nuclepore, 0.22 μm) and counted under an epifluorescence microscope (Zeiss Axio Imager Z1).

2.6 Biometry of *C. nodosa* and epiphytic macroalgae

The material from each quadrat was washed under running seawater to remove sediment. From each quadrat algae, leaves and rhizomes with roots were separated. The length of the longest leaf on each shoot was measured and the shoots were counted. Species of macroalgae were determined, and their coverage was estimated according to the Braun-Blanquet scale. Separated samples were washed with filtered and autoclaved seawater, weighed, dried at 60 °C for 48 h and re-weighed. The dry mass was calculated per area (g m^{-2}).

2.7 Granulometric composition of the sediment and its organic matter content

For granulometric analysis of the sediment, each sample was wet sieved through a set of seven standard ASTM sieves (4-, 2-, 1-, 0.5-, 0.25-, 0.125-, 0.063-mm mesh size). The fraction that passed through the 0.063-mm sieve was collected and analyzed following the standard sedigraph procedure (Micromeritics, 2002). The material that was retained on the sieves was dried and weighted. The data obtained by both techniques were merged to obtain a continuous grain size range and analyzed with the statistic package Gradistat v 6.0. Sediments were classified according to Folk (1954). The sediment permeability was calculated based on median grain size (d_g) following the empirical relation by Gangi (1985). The organic matter content was determined as ignition loss after heating dried sediment sections at 450°C for 4 h in a muffle furnace.

https://doi.org/10.5194/bg-2019-484
Preprint. Discussion started: 21 January 2020
© Author(s) 2020. CC BY 4.0 License.

2.8 Oxygen (O_2), hydrogen sulfide (H_2S) and redox potential (Eh) profiling

The microprofiles of O_2, H_2S and Eh were measured on intact cores immediately after sampling using a motorized micromanipulator (MMS9083) equipped with microsensors OX-100 and H_2S-200, redox microelectrode RD-200 coupled with reference electrode REF-RM (Unisense A/S, Denmark). Prior to the measurements, the OX-100 microsensor was calibrated using a two-point oxic – anoxic calibration; H_2S-200 was calibrated in fresh Na_2S solutions using eight-point calibration (1μM - 300 μM in a de-oxygenated calibration buffer (NaAc/HAc, pH <4); RD-200 with REF-RM was calibrated using two point calibration by simultaneous immersion of electrodes in quinhydrone redox buffers prepared in pH 4 and pH 7 buffers, all according to the manufacturer's recommendation. During measurements, sediment cores were placed in a pool filled with seawater from the sampling site to maintain *in situ* temperature. From July to October 2017 H_2S was measured spectrophotometrically in pore waters (Cline, 1969) squeezed out by centrifugation from each section (5 mm) of the sediment cores.

2.9 Total lipids, fatty acid composition and elemental sulfur (S^0)

Lyophilized samples of seagrass tissues, macroalgae, sediment or particulate matter were weighed and extracted into a solvent mixture of dichloromethane/methanol (DCM: MeOH, 2:1) in an ultrasonic bath at 35°C with three solvent mixture changes. The extracts were pooled and separated into layers by addition of 0.9% NaCl solution. Lower DCM layers (containing lipids) were released over Na_2SO_4 anhydride, collected in pre-weighed round bottom flasks and evaporated to dryness using rotavapor. After evaporation, flasks were re-weighed, and total lipid concentrations (TL, mg g^{-1} DW) were calculated from the difference in weight. For fatty acids determination, lipid extracts were saponified (1.2 M NaOH in methanol), acidified (6 M HCl), methylated (14% BF_3 in methanol) and extracted into DCM.

Fatty acid methyl esters (FAME) were analyzed by Agilent gas–liquid chromatography (GLC) 6890 N GC System equipped with a 5973 Network Mass Selective Detector, capillary column (30 m x 0.3 mm x 0.25 μm; cross-linked 5 % phenylmethylsiloxane) and ultra-high purity helium as the carrier gas. The GLC settings were as follows: programmed column temperature rise from 145°C by 4°C/min to 215°C, then by 1°C/min to 225°C and finally by 4°C/min to 270°C at constant column pressure of 2.17 kPa. Retention times, peak areas and mass spectra were recorded on the ChemStation Software. FAME were identified by mass spectral data and family plots of an equivalent chain length (ECL) for GC standards. Applied GC standards were: FAME mix C18–C20, PUFA1, PUFA3 standards (Supelco/Sigma-

https://doi.org/10.5194/bg-2019-484
Preprint. Discussion started: 21 January 2020
© Author(s) 2020. CC BY 4.0 License.

Aldrich, Bellefonte, PA, USA); C4–C24 FAME standard mix, cod liver oil and various individual pure standards (Sigma, Neustadt, Germany).

The following indices of fatty acid profiles were calculated: saturated fatty acids (SAT), monounsaturated fatty acids (MUFA), polyunsaturated fatty acids (PUFA) and the unsaturation degree (UND). UND was employed to evaluate the degree of organic matter degradation due to more susceptibility of unsaturated, particularly polyunsaturated, components to degradation and calculated according to the formula [1*(% mono-)+2*(% di-)+3* (% tri-)+4*(% tetra-)+5*(% penta-)+6*(% hexa-enoic)]/% SAT (Pirini et al., 2007). To evaluate the input of terrestrial organic matter relative to that of marine origin in particulate matter, the terrestrial to aquatic acid ratio (TAR= C24+C26+C28 / C12+C14+C16) was used (Cranwell et al., 1987; Bourbonniere and Meyers, 1996).

In FAME chromatograms elemental sulfur (S^0), eluted as S_8 (m/z 256), was identified by comparison of retention time and characteristic fragment ions in samples and standard solutions. The concentration of S^0 was estimated on the base of the calibration curve prepared for standard solution of S_8 (Aldrich, Germany) in cyclohexane (2-20 mg L^{-1}). The calibration curve was determined under the same GLC settings as FAME. Limit of detection (LoD) and limit of quantitation (LoQ) were calculated from the parameters of the calibration curve constructed on the basis of the 3 lowest concentrations in 3 replicates. LoD and LoQ (0.92 mg L^{-1} and 2.80 mg L^{-1}, respectively) were more than twice the values obtained by Rogowska et al. (2016) probably due to higher injector and column temperature used in this study than they proposed as optimal for S determination.

2.10 Data analyses

A multivariate analysis, hierarchical clustering and K-means methods (Systat 12) was applied to group *C. nodosa* above- and below-ground tissues according to the similarity of their fatty acid profiles and indices, i.e., physiological condition during the investigated period.

Sediment data were analyzed for two groups of sediment layers, the upper layer (0- 4 cm) where most of rhizomes and roots are located, and the lower layers (5-7 cm). Differences between vegetated and non-vegetated sediment samples in each sediment layer were tested by one-way ANOVA. Correlations among parameters were tested using the Pearson's correlation coefficient (r). The level of statistical significance was $p < 0.05$. A multivariate principal component analysis (PCA, Primer 6) was applied to identify the most important variables explaining differences between vegetated and non-vegetated sediments. Correlation matrices were constructed using variables: H_2S, Eh, O_2, S^0, PA, TL and UND. All variables were

https://doi.org/10.5194/bg-2019-484
Preprint. Discussion started: 21 January 2020
© Author(s) 2020. CC BY 4.0 License.

normalized due to their different scales. Only the principal components with eigenvalues >1 were considered.

3 Results

3.1 Water column

3.1.1 Environmental variables

During summer of 2017 daily means of sea-bottom temperature in *C. nodosa* meadow ranged between 26°C and 28°C. During autumn seawater temperatures decreased below 12°C until the end of December. The coldest period was recorded at the beginning of March lasting only for a few days (min. 8.62°C). From April to mid-July 2018, temperature increased with moderate fluctuations to the maximum of 29.26°C recorded in August 2018 (Fig. 1a).

Concentrations of inorganic nutrients and Chl *a* were generally low. The highest concentrations (DIN: 8.27 µM; PO_4: 0.18 µM; SiO_4: 9.82 µM; Chl *a*: 0.89 µg L^{-1}) associated with the lowest salinity (34.2) were found in September 2017 (Table S1). The abundance of prokaryotes (2.6-11.3 x 10^5 cell mL^{-1}) varied seasonally and significantly correlated to seawater temperatures ($r = 0.618$; $p < 0.05$). In contrast, salinity (S: 34.2 - 38.5) and concentrations of particulate matter (PM: 3.84 - 14.21 mg L^{-1}) showed irregular variations (Fig. 1b) and a significant opposite trend ($r = -0.630$; $p < 0.05$).

The particulate lipids exhibited the highest unsaturation degree (UND) during summer/early autumn 2017 and small increases of UND in April and September/October 2018 (Fig. 1c). UND was significantly correlated with Chl *a* ($r = 0.603$; $p < 0.05$). In contrast, terrestrial to aquatic ratio (TAR) considerably increased in April and was the highest in August 2018 (Fig. 1c). TAR was negatively correlated to UND ($r = -0.644$, $p < 0.05$) and positively to particulate matter ($r = 0.641$, $p < 0.05$). Although PUFA with 18 C atoms made the largest contribution to the total PUFA pool, C20 PUFA, mainly of phytoplankton origin, showed a similar trend as observed for UND (Fig. S1, Table S2).

3.2 *Cymodocea nodosa* meadow

3.2.1 Biometry

C. nodosa leaves and shoots reached the highest biomass (285.3 ± 57.4 g m^{-2}), length (102.4 ± 26.6 mm) and shoot density (3703±334 shoots m^{-2}) in October 2017 (Fig. 2a). After the appearance of the regular vegetation minimum in November 2017, biometric indices further decreased reflecting the decay of the meadow in summer 2018. In August 2018, only yellow to brownish leaves on sparse shoots were collected (4.5 ± 1.3 g m^{-2}, 5.4 ± 1.3 mm and 30 ± 35

https://doi.org/10.5194/bg-2019-484
Preprint. Discussion started: 21 January 2020
© Author(s) 2020. CC BY 4.0 License.

shoots m^{-2}). In September and October 2018, no shoots or leaves were observed (Fig. 2a). The biomass of rhizomes and roots reached also its maximum in October 2017 (599.7 ± 36.8 g m^{-2}). In contrast to leaves and shoots, the belowground biomass was stable until March 2018 when a decline was observed that continued until October 2018 (30.5 ± 6.8 g m^{-2}) (Fig. 2a).

3.2.2 Total lipid (TL) concentrations and fatty acid composition

TL in the *C. nodosa* aboveground tissue (6.7 - 25.3 ± 2.4 mg g^{-1} DW) increased until February 2018, when maximum TL concentrations were measured (Fig. 2b). Thereafter, TL concentrations decreased until August 2018. During this period, the belowground TL concentration (6.3 ± 1.9 – 15.9 ± 1.1 mg g^{-1} DW) was generally lower than the aboveground TL concentrations and the trend was similar to that of leaves. The minimum concentrations of TL were observed in September 2018, while in October 2018, concentrations similar to that measured in October 2017 were observed (Fig. 2b).

The major fatty acid components in *C. nodosa* tissues were palmitic (C16:0) amongst the saturated (SAT) and oleic (C18:1n-9) in monounsaturated fatty acids (MUFA). In the aboveground tissue, the main polyunsaturated fatty acids (PUFA) were α-linolenic (C18:3 n-3, ALA) and linoleic (C18:2 n-6, LA), while in the belowground tissue LA was dominant (Fig. 2b). The dynamics of UND in the aboveground tissue was principally influenced by changes in ALA and LA. LA/ALA ratios were < 1 from July 2017 to March 2018, and > 1 from April to July 2018 (Fig. 2b). In August 2018, the LA/ALA ratio was infinite due to the absence of ALA (Fig. 2b). Elemental sulfur (S^0) was detected only in decaying leaves in August 2018 (0.21 mg g^{-1} DW). In the belowground tissue, S^0 was detected in all samples (Fig. 2b). Higher concentrations were measured during summer 2017 (up to 0.39 ± 0.06 mg g^{-1} DW). S^0 increased from minimum concentrations in April (0.02 ± 0.01 mg g^{-1} DW) until September 2018 reaching 1.42 mg g^{-1} DW (Fig. 2b).

According to the fatty acid profiles, *C. nodosa* leaves were classified in three groups, except for the leaves collected in August 2018 (Fig. 3). The most distinguishing features specifying physiological differences between Group 1 (July - October 2017 and February - March 2018), Group 2 (November - December 2017 and April - May 2018) and Group 3 (June and July 2018) were decreasing mean values of PUFA, UND, ALA and LA and increasing means of SAT and the proportion of long-chain saturated fatty acids (C ≥ 24). In the ungrouped leaves from August 2018 ALA was not found, PUFA and UND were at a minimum, while SAT and C ≥ 24 at a maximum (Table S3). Three groups of rhizomes and roots (Group 1: July - October 2017 and February - March 2018; Group 2: November -

https://doi.org/10.5194/bg-2019-484
Preprint. Discussion started: 21 January 2020
© Author(s) 2020. CC BY 4.0 License.

December 2017 and April - May 2018 and Group 3: (June - October 2018) showed similar characteristics to the groups 1, 2 and 3 of related leaves (Table S4).

3.2.3 Epiphytic macroalgae

From July 2017 to February 2018 different taxa of macroalgae belonging to the three phyla Chlorophyta (*Halimeda tuna*, *Dasycladus vermicularis*, *Cladophora prolifera*, *Udotea petiolata*), Rhodophyta (*Rytiphlaea tinctoria*, *Peyssonnelia* spp, *Gelidium* sp.) and Ochrophyta (*Dictyota dichotoma*) were covering the meadow in varying proportions and abundances (Fig. 4). After March 2018, when only few individuals of *Peyssonnelia* sp. were found, macroalgae were no longer present in the *C. nodosa* meadow.

Although the fatty acid profiles of macroalgal communities were highly variable, the contribution of 18- and 20 PUFA to the total PUFA pool generally depended on the prevailing phyla and their characteristic PUFA pattern. The algae belonging to Rhodophyta and Ochrophyta are richer in 20 PUFA (C20:5n-3, C20:4n-6), while Chlorophyta are generally showing prevalence of 18 PUFA (C18:3n-3, C18:2n-6) (Schmid et al., 2014). Furthermore, their contribution to biomass varied due to large differences in morphology, which most likely also contributed to the variability of fatty acid profiles. 18 PUFA and 20 PUFA showed the highest contribution to the total PUFA pool during the dominance of Chlorophyta and Rhodophyta in the macroalgal community, respectively. In most samples, the lowest contribution to the total PUFA pool was observed for 16 PUFA and 22 PUFA (Fig. S2).

3.3 Sediment

3.3.1 Granulometric composition

According to the granulometric composition, median grain sizes (d_g) and permeability (k) the vegetated and non-vegetated sediments were classified as slightly gravelly sandy mud (g)sM, fine grained ($d_g < 165$ µm) and low permeable to impermeable sediment ($k < 2 \cdot 10^{-11}$ m^2). In general, the *C. nodosa* sediment consisted of a significantly higher proportion of sand (Sa), and lower proportion of silt (Si) and clay (C) (Sa, 41.11 ± 4.34 %; Si, 46.44 ± 2.86 %; C, 9.63 ± 2.76 %) in comparison to non-vegetated sediment (Sa, 20.53 ± 10.49 %; Si, 53.24 ± 6.76 %; C, 23.29 ± 4.86 %). The median grain size and permeability in *C. nodosa* sediment (d_g, 37.51 ± 17.97 µm, k, $1.22 \cdot 10^{-12} \pm 1.13 \cdot 10^{-12}$ m^2) were significantly higher than in non-vegetated sediment (d_g, 10.86 ± 5.34 µm; k, $1.04 \cdot 10^{-13} \pm 1.02 \cdot 10^{-13}$ m^2). The upper layers of both cores (0 - 4 cm) had larger particles, while the lower layers (5 - 8 cm) showed a uniform distribution of smaller grain sizes (Fig. 5).

https://doi.org/10.5194/bg-2019-484
Preprint. Discussion started: 21 January 2020
© Author(s) 2020. CC BY 4.0 License.

3.3.2 O_2, E_h, H_2S and S^0

Oxygen concentrations (O_2) in the bottom water of the *C. nodosa* meadow varied in a wide range (0 µM - 171.4 ± 17.6 µM) and generally followed the O_2 saturation trend (Fig. 6a). From May to June 2018, O_2 decreased below 62.5 µM, considered as severe hypoxia (Vaquer-Sunyer and Duarte 2008) and was completely depleted in July 2018 (Fig. 6a). From August to October 2018, O_2 increased again. The variations of O_2 in the bottom water of the non-vegetated sediment were similar to those in the *C. nodosa* meadow albeit generally higher (79.4 ± 10.4 µM – 212.2 ± 33.4 µM) than in the vegetated sediment except for September and October 2018 (Fig. 6a).

In general, O_2 penetration depth in the vegetated and non-vegetated sediment co-varied with the O_2 concentration in the bottom layer, penetrating deeper when its concentration in the bottom water was higher (Fig. 6b). In the vegetated sediment, O_2 was mainly depleted down to 1 cm of depth. In the non-vegetated sediment, the oxygen penetration depth was up to 4 times higher than in vegetated sediments, except for the period from August 2018 to October 2018 when the penetration depths were similar (Fig. 6b).

The thickness of the oxic (Eh > 150 mV) and suboxic (150 mV > Eh > 0 mV) layers in the vegetated sediment increased from July 2017 (~ 0.5 cm) to March 2018 (~ 4 cm), and decreased progressively from April (~ 0.8 cm) towards the surface in July 2018, when the entire sediment core was anoxic (Eh < 0). From August (~ 1 cm) to October 2018 (~ 2.5 cm) the oxic and suboxic layer thickness increased again (Fig. 7). Oxic conditions (Eh > 0) generally reflected O_2 concentrations in the bottom waters. The dynamics of Eh in non-vegetated sediment were similar to those in the vegetated sediment. However, the thickness of the oxic layer was considerably larger than in the vegetated sediment. Reducing conditions (Eh < 0) were only recorded in July and August 2017 (Fig. 7).

Concentrations of free H_2S in the pore water of the vegetated sediment generally increased with depth creating an accumulation zone mainly within the upper sediment layers (1 - 4 cm) (Fig. 7). From July to November 2017, H_2S concentrations increased up to 120 µM (at 4 - 5 cm). In December 2017, H_2S was low and uniformly distributed throughout the core (< 5 µM). H_2S concentrations increased and the accumulation layer was ascending from March (up to 34.2 ± 12.8 µM; 5 - 7 cm) to April 2018 (up to 177.2 ± 125.1 µM; 3.5 - 4.5 cm). During May 2018 (up to 107.8 ± 75.9 µM; 2.5 - 4 cm), June (up to199.0 ± 6.3 µM; 1.5 - 6 cm) and July (up to 210.1 ± 138.9 µM; bottom water - 6 cm) a propagation of the accumulation zone was observed in addition to an increase in H_2S (Fig. 7). In August 2018 (up to 1164.1 ± 702.1 µM; bottom water - 7 cm) extremely high concentrations over the entire sediment core were

https://doi.org/10.5194/bg-2019-484
Preprint. Discussion started: 21 January 2020
© Author(s) 2020. CC BY 4.0 License.

recorded. In September and October 2018, H_2S concentrations decreased (down to 140.0 ± 25.3 and 72.7 ± 52.7 µM; bottom water - 7 cm and 1 - 7 cm, respectively). In the non-vegetated sediment, H_2S depth profiles were similar to those in vegetated sediments, but the concentrations were generally lower, except for the summer of 2017 when the concentrations were comparable but the accumulation zones deeper (Fig. 7).

S^0 mainly occurred in oxic (Eh > 150 mV) and suboxic (150 mV > Eh > 0 mV) layers of both, vegetated and non-vegetated sediments (Fig. 7). Generally, the ranges of approximated S^0 concentrations in vegetated sediment ($8.5\cdot10^{-5}$ - 0.39 mg·g^{-1} DW ~ $2.6\cdot10^{-3}$ - 12.1 µmol·g^{-1} DW), except for the extreme value in April 2018 (0.99 mg·g^{-1} DW ~ 30.8 µmol·g^{-1} DW), were similar to those found at the non-vegetated sites ($2.9\cdot10^{-4}$ – 0.28 mg·g^{-1} DW ~ $9.2\cdot10^{-3}$ – 8.9 µmol·g^{-1} DW).

3.3.3 Prokaryotic abundance

Prokaryotic abundance varied largely in vegetated (2.1 - 39.9· 10^7 cells g^{-1} fresh weight, FW) and non-vegetated sediments (3.7 - 24.1·10^7 cells g^{-1} FW). Prokaryotic abundance was significantly higher in the upper than the lower layers of vegetated ($F = 40.553$, $p < 0.05$) and non-vegetated ($F = 52.531$, $p < 0.05$) sediments (Fig. 8). Prokaryotic abundance showed significant monthly changes in the upper ($F = 3.053$, $p < 0.05$) and lower layer ($F = 5.035$, $p < 0.05$) of vegetated sediments, in contrast to both layers of non-vegetated sediments ($p > 0.05$). Prokaryotic abundances were significantly higher in the upper layers ($F = 44.577$, $p < 0.05$) and significantly lower in the lower layers ($F = 5.986$, $p < 0.05$) of vegetated than in the respective layers of non-vegetated sediments (Fig. 8). In the upper sediment layer, prokaryotic abundances were significantly higher in the vegetated than in the non-vegetated sediments from July to October 2017 and from June to August 2018 (Fig. 8). In the lower layers of vegetated sediments, prokaryotic abundance was significantly higher than in the non-vegetated sediments in October 2017 and in August and September 2018 (Fig. 8).

3.3.4 Organic matter, total lipids and fatty acid composition

The concentrations of organic matter (OM) and total lipids (TL) were highly correlated in vegetated (OM: 37.6 - 231.1 mg/g DW, TL: 0.15 - 2.75 mg/g DW; $F = 214.172$, $p < 0.05$) as well as in non-vegetated sediments (OM: 56.7 - 160.3 mg/g DW, TL: 0.33 - 2.39 mg/g DW; $F = 45.569$, $p < 0.05$). OM and TL generally decreased with depth and exhibited similar changes throughout the investigated period with significantly higher concentrations in upper than in lower sediment layers ($p < 0.05$) (Fig. 9).

https://doi.org/10.5194/bg-2019-484
Preprint. Discussion started: 21 January 2020
© Author(s) 2020. CC BY 4.0 License.

In the vegetated sediment, TL showed significant monthly changes in the upper ($F = 11.418$, $p < 0.05$) and lower sediment layers ($F = 3.186$, $p < 0.05$), in contrast to both layers of non-vegetated sediment ($p > 0.05$). From July to October 2017, in the upper layer of vegetated sediments, TL was significantly higher than in non-vegetated sediments (Fig. 9). From November 2017 onwards, TL decreased slightly until April 2018, reaching similar concentrations as TL in non-vegetated sediments (Fig. 9). TL concentrations decreased markedly in May and continued until August 2018. During that period, TL in vegetated sediments was significantly lower than in non-vegetated sediments. In September and October 2018, TL concentrations in vegetated sediments were similar to those in non-vegetated sediment (Fig. 9).

The fatty acid composition of vegetated and non-vegetated sediments was similar and in both layers characterized by the prevalence of SAT (vegetated upper: 71.2 - 90.4%, lower: 75.9-89.1%; non-vegetated upper: 71.2-80.7%, lower: 78.2-82.5%) over MUFA (vegetated upper: 7.6-22.9%, lower: 9.0-19.9%; non-vegetated upper: 17.8-24.1%, lower: 15.3-18.2%) and PUFA (vegetated upper: 1.9-6.9%, lower: 1.9-5.1%; non-vegetated upper: 1.7-4.8%, lower: 1.7-3.9%). The trends of the monthly changes in UND were similar in both layers of both sediment types. Those variations were less pronounced in the non-vegetated sediment where UND varied in narrower ranges in both layers (upper: 0.26-0.51, lower: 0.23-0.33) than in vegetated sediment (upper: 0.13-0.57, lower: 0.14-0.37). From July to October 2017 and in April 2018, UND was higher in the upper layers of vegetated sediment than in non-vegetated one, while from November 2017 to March 2018, UNDs of both sediments were lower than in previous period (Fig. 9). From June to August 2018, UND decreased considerably in vegetated sediment, being lower than in non-vegetated sediments. During September and October 2018, an increase of UND was observed in both sediments. In the lower layers, UNDs were similar, except for July and August 2018 when a considerable decrease of UND was observed in vegetated sediments (Fig. 9).

The proportions of PUFAs with chain lengths of 16, 18, 20, and 22 C atoms within the PUFA pool were similar between the respective layers of both sediments. Throughout the study period, the highest contribution of 18PUFA originated from *C. nodosa* detritus and Chlorophyta was observed (Fig. S3, Table S2). From July to October 2017, April to May 2018 and September to October 2018, a contribution of 20PUFA attributed to phytoplankton and Rhodophyta was also detected. 16PUFA and 22PUFA accounted for the smallest contribution to the PUFA pool and were found in seston and macroalgae (Fig. S3, Table S2).

https://doi.org/10.5194/bg-2019-484
Preprint. Discussion started: 21 January 2020
© Author(s) 2020. CC BY 4.0 License.

The similarities between the sediments were also observed in the contribution of the main SAT components to the SAT pool from July 2017 to March 2018 and from September to October 2018 (Fig. S3, Table S2). From April to August 2018, an increase of the long-chain (C≥ 24) and common (C16:0 + C18:0) fatty acids followed by the decrease of bacterial fatty acids (BACT) contribution to the SAT pool was observed in both layers of the vegetated sediment. In contrast, the contribution of these components to the SAT pool was fairly invariable in non-vegetated sediments during the same period (Fig. S3, Table S2).

3.3.5 Relationship between different physicochemical parameters

The relationships between H_2S, O_2, TL, S^0, PA, Eh and UND in vegetated and non-vegetated sediment are shown in the principal component analysis, where PC1 explained 42.5 % and PC2 14.4 % of variability (Fig. 10). The loadings for positive relationships were obtained for H_2S (0.298) on PC1 and Eh (0.541) and O_2 (0.327) on PC2. For the negative relationships, the loadings were for TL (-0.534), UND (-0.494), S^0 (-0.388), Eh (-0.327), PA (-0.296) and O_2 (-0.191) on PC1, and H_2S (-0.536), S^0 (-0.485), TL (-0.165) and UND (-0.221) on PC2.

PC1 separated most of the upper sediment layers (July 2017 - May 2018, September - October 2018) according to the higher concentrations of TL and S^0, higher UND and more positive Eh from the most of the lower layers and upper layers of vegetated sediments (June - August 2018) with increased H_2S concentrations. On PC2, the vegetated was separated from the non-vegetated sediment due to higher concentrations of H_2S, S^0 and more negative Eh, which characterized vegetated sediments during almost the entire study period. The extreme concentrations of S^0 and H_2S found in the upper layer in April and the lower layer in August 2018, respectively, were responsible for the considerable separation of these layers from all other vegetated layers (Fig. 10).

4 Discussion

Saline Bay is a shallow, highly dynamic coastal area characterized by frequent turbid waters due to the combined effect of land run-off and wind-driven resuspension of fine sediment. Nutrients and Chl *a* (as a proxy for autotrophic biomass) varied in the ranges characteristic for the oligotrophic coastal waters off Rovinj (Ivančić et al., 2018). The increases in particulate matter concentration were associated with freshwater input, while their enrichment with unsaturated fatty acids deriving from phytoplankton was observed during the increases of autotrophic biomass. However, only in September 2017, this increase was supported by nutrients from the water column, while all other less pronounced increases were most likely connected to bottom waters where phytoplankton could have been supplied with nutrients made available through sediment resuspension. In accordance, increases in the particulate lipid matter of terrigenous origin have been observed, being generally elevated from April to August 2018. Therefore, during this investigation the dynamics of the particulate matter was most likely under the combined influence of terrigenous input and sediment resuspension, including detritus from the *C. nodosa* meadow.

In temperate Mediterranean coastal waters *C. nodosa* meadows show a clear unimodal annual growth cycle, reaching maximum development in summer, and minima during winter and a particularly active growth phase in spring (Terrados and Ross, 1992; Zavodnik et al., 1998; Agostini et al., 2003). In Saline Bay, the maximum growth was shifted towards early autumn. This shift was most likely due to the prevalence of massively grazed leaves during July and August 2017, suggesting an intense grazing activity in the meadows, which probably decreased during September and October 2017. A minimum growth occurred during late autumn/winter, as commonly observed. However, during the spring 2018, phenological parameters continued to decrease in spite of established favorable environmental conditions for growth, i.e., increase in water temperature, intensity and period of solar radiation. This decrease continued until the complete extinction of the aboveground tissue in August 2018. The belowground tissue followed a similar trend, but with less expressed changes. Still, their recognizable remnants were found after the loss of the aboveground tissues.

During the summer/early autumn 2017 and winter 2018, an adaptation of *C. nodosa* leaves to the decreasing solar radiation and temperature occurred, respectively. In both periods, an increase in unsaturation degree (primarily due to ALA increase) in order to increase the membrane fluidity was observed. From July to October 2017, the temperature of the water column was still optimal for elongation of the leaves and biomass increase, while the ambient light intensities were continuously decreasing. An additional reduction of available light might occur from the self-shading effect due to high canopy biomass, and/or shading due to epiphytic macroalgae growth and turbidity of the water column. Desaturation of low and fairly invariable lipids during the most active growth phase suggested an increase in the membrane fluidity to optimize photosynthetic activity under low light conditions. Such physiological adaptation as a response to low light availability was found in seagrasses living along a depth gradient (Beca-Carretero et al., 2019) and macroalgae in contrasting seasons (Schmid et al., 2014). During the winter, data indicate a progressive trend toward highest total lipids as well as the proportions of PUFA. Rapid desaturation of increasing lipids could be attributed primarily to a sharp and continuous decrease in water temperature. An increase in

© Author(s) 2020. CC BY 4.0 License.

the level of PUFA is considered to provide a mechanism for the thermo-adaptive regulation of membrane fluidity and cold resistance in algae and plants (Terrados and Lopezjimenez, 1996; Iveša et al., 2004; Upchurch, 2008).

In contrast, in late autumn 2017 and spring 2018, the decrease in PUFA and UND indicated a reduced fluidity and activity of photosynthetically active membranes. The lower fluidity reduces proton leakage through the thylakoid membranes and energy consumption for their maintenance (Quigg et al., 2006; Wacker et al., 2016). The reduced photosynthetic activity was associated with a decreased abundance of shoots and aboveground biomass. During the period of reduced growth and shedding leaves and shoots the plant further balances metabolic requirements and mobilize energy from the carbohydrate reserves stored in the belowground tissue (Alcoverro et al., 2001; Lee et al., 2007). However, major differences are observed between the two periods indicated by the LA/ALA ratios. During November and December, LA and ALA proportionally decreased by keeping their ratio < 1, while during April and May ALA decreased while LA remained stable. The resulting LA/ALA > 1 suggests a decrease in the conversion of LA to ALA, which occurs in conditions of light reduction (Harris and James, 1965). This finding apparently contradicts the adaptation to low light conditions observed during *C. nodosa* healthy and regular growth and suggests the reduction of light below the minimum requirements for *C. nodosa* survival. Such conditions of light deprivation existed in April 2018, when the plant had been most probably exposed to increased siltation, due to a rise in terrigenous input combined with resuspension of sediment provoking elevated autotrophic growth. The intensive siltation is associated with the increased light attenuation, both through the direct shading effect of suspended sediments and through the promotion of phytoplankton and epiphyte growth by the associated increase in nutrients (Terrados et al., 1998; Halun et al., 2002; Brodersen et al., 2015). Therefore, the increase in seawater turbidity and considerable sediment re-deposition on the leaves might have severely impaired the light availability and slowed down the plant's photosynthetic activity. When the minimum light requirements (~14% of incidence light) are not met, *C. nodosa* intensely sheds leaves and shoots, while at light level of < 1% of surface solar radiation the plant dies off (Collier et al., 2012). This reduced light condition apparently persisted until May 2018 and most likely prevented the re-establishment of photosynthesis and *C. nodosa* continued to shed shoots and leaves.

During June and July, the increase in LA/ALA ratio in the leaves and overall saturation of decreasing lipids in above- and below-ground tissues indicated a sudden and significant deterioration of the physiological conditions of *C. nodosa*. Additionally, the loss of leaf tissue

https://doi.org/10.5194/bg-2019-484
Preprint. Discussion started: 21 January 2020
© Author(s) 2020. CC BY 4.0 License.

negatively impacted the photosynthetic carbon fixation and therefore oxygen production, including the transport of oxygen to belowground tissue (Lee and Dunton, 1997; Lee et al., 2007). The belowground tissue that was not supported by photosynthetically derived oxygen became anaerobic. The induced anaerobiosis most likely caused a complete inhibition of the fatty acid desaturation chain (Harris and James, 1965) and a permanent breakdown of photosynthesis leading to the final decay of the aboveground biomass in August 2018. As a result, the reduced renewal and storage of energy reserves in the belowground tissue led to a considerable depletion of reserves and loss of biomass.

In a healthy seagrass meadow, the oxygen generated by seagrass photosynthesis is transported to belowground tissues to maintain an oxic microsphere around roots and rhizomes, re-oxidize sulfide to non-toxic S^0, thus preventing an invasion of H_2S into the plant (Pedersen et al., 1998; Holmer et al, 2005). Due to rapid oxygen depletion for respiratory needs and low storage capacity of lacunae, oxic conditions in belowground tissues are partially maintained by oxygen diffusing from the water column into belowground tissue (Pedersen et al., 1998; Greve et al., 2003; Sand-Jensen et al., 2005). An oxic microsphere around the seagrass roots stimulate the growth of endosymbiotic sulfide-oxidizing prokaryotes (Jensen et al., 2007), which are regular members of the seagrass microbiome (Ugarelli et al., 2017; Fahimipour et al., 2017). S^0 was found in the *C. nodosa* belowground tissue during the entire investigation period, as already observed in seagrasses living in sulfidic sediments (Holmer and Hasler-Sheetal, 2014; Hasler-Sheetal and Holmer, 2015). However, from July 2017 until March 2018, it seems that the plant was sufficiently supplied with oxygen produced either by photosynthesis and/or supplied by diffusion from the well-oxygenated water column. This probably ensured the complete re-oxidation of the potentially intruding sulfide preventing root anoxia. As photosynthesis and therefore oxygen production were already reduced in April 2018, the maintenance of the oxic rhizosphere and the internal O_2 partial pressure in the lacunae further depended mainly on the diffusion of O_2 from the water column. From April to June 2018, O_2 in the bottom water drastically decreased. Due to poor supply, O_2 content of the belowground tissue was too low to maintain the oxic microenvironment and therefore, the plant tissues became potentially accessible to sulfide intrusion (Pedersen et al., 2004). To reach the leaves, sulfide invasion has to exceed belowground tissue oxidation capacity and pass through these tissues, invading the meristems located at the base of the leaves, where sulfide toxicity can have drastic effects on shoot growth and survival (Greve et al., 2003; Frederiksen et al., 2008). In July 2018, the bottom waters were completely depleted in O_2 and the whole plant probably exposed to H_2S. H_2S

inhibit cytochrome c oxidase by binding to regulatory sites on the enzyme, reducing the rate of cellular respiration and leading to the chemical asphyxiation (Nichols et al., 2013). In August 2018, the inflow of freshwaters re-oxygenated the bottom waters enabling H_2S oxidation in leaves, which were, however, already in an advanced stage of decomposition. During September and October 2018, the penetration of O_2 from the water column gradually led to the recovery of belowground tissue.

In addition to plant activity, sulfide intrusion into seagrasses is controlled by sediment biogeochemistry and environmental conditions (Frederiksen et al., 2006), while sulfide concentration in sediments is determined by the rate of sulfate reduction, which in turn depends on the amount of organic matter and temperature (Moeslund et al., 1994). Organic matter and closely correlated total lipids in the sediment of *C. nodosa* rooted area changed significantly throughout the investigated period, in contrast to organic matter in non-vegetated sediment. Nevertheless, considerable but the co-varying unsaturation degree suggests similarity in the quality and degradation degree of lipid matter at both, the vegetated and the non-vegetated sites. This covariation indicates an important contribution of detritus imported from the meadow as a source of organic matter for prokaryotes in non-vegetated sediments. Close coupling between the seagrass meadow and non-vegetated sites could be expected due to their proximity and lower organic content of the non-vegetated sediment, which should enhance the dependence of prokaryotes on the imports of seagrass detritus from the adjacent meadows (Holmer et al., 2004). Moreover, the non-vegetated sediment in Saline Bay could readily support the adsorption of imported organic material due to a higher proportion of mud (silt and clay) and considerably lower median grain size in comparison to the *C. nodosa* sediment.

C. nodosa sediment was significantly enriched with organic matter, characterized by a higher contribution of unsaturated, more labile components, in comparison to the non-vegetated sediment layer only during abundant growth of meadow. Also, sestonic material from the water column is efficiently trapped and accumulates within the meadow (Gacia and Duarte, 2001), representing an additional source of labile components derived from macroalgae and *C. nodosa* leaves. Such easily utilizable organic matter, including dissolved monomeric carbohydrates, leaching out during decomposition of *C. nodosa* leaves stimulates prokaryotic growth (Peduzzi and Herndl, 1991). This effect could be observed, as prokaryotic abundance was higher in *C. nodosa* sediments (Fig. 8). In contrast, the lower unsaturation of lipid matter in the non-vegetated sediment can be explained by its higher instability.

https://doi.org/10.5194/bg-2019-484
Preprint. Discussion started: 21 January 2020
© Author(s) 2020. CC BY 4.0 License.

Resuspension and a wider oxic layer could have further suppressed the preservation of reactive and more labile organic matter in comparison to the *C. nodosa* sediment.

The relatively low accumulation of H_2S (< 30 μM) during the summer and early autumn 2017 indicated that H_2S was apparently rapidly recycled within the rooted area via re-oxidation by O_2 to S^0 and/or removal by precipitation with iron compounds. Most of S^0 was found in oxic layers or suboxic/anoxic boundaries, but also anoxic layers in July and October 2017. The oxidation of H_2S could occur spontaneously by chemical reaction with free oxygen or mediated by sulfide-oxidizing bacteria (Jørgensen, 1977). Usually S^0 is the most abundant sulfide oxidation intermediate, and it accumulates to higher concentrations than other more reactive compounds (e.g. polysulfide, thiosulfate, tetrathionate, sulfite; Zopfi et al., 2004). In Saline Bay sediment S^0 occurs in ranges typical for sulfidic coastal sediments (Troelsen and Jørgensen, 1982; Panutrakul et al., 2001; Pjevac et al., 2014). During the active growth of *C. nodosa*, the rhizosphere surrounding sediment was well supplied with photosynthetically produced oxygen due to radial oxygen leakage. Therefore, in addition to free oxygen available in pore waters, both, biotic and abiotic re-oxidation of sulfide was most likely supported by the oxygen supplied via the release from the root to the surrounding sediment (Holmer et al., 2006). Generally, thermodynamic and kinetic considerations suggest that biological oxidation far exceeds chemical oxidation of sulfide in most environments (Wasmund et al., 2017). Moreover, abundant sulfide oxidizing prokaryotes have been detected in marine sediments surrounding or attaching to seagrass roots (Cucio et al., 2016; Fahimipour et al., 2017).

In November, due to the degradation of organic matter and reduced oxygen production and leakage in the rooted zone caused by *C. nodosa* senescence, the re-oxidation capacity of the sediment was greatly decreased. This resulted in considerable accumulation of H_2S (> 100 μM) which extended up to the sediment surface. During winter and early spring, H_2S production generally decreased, likely due to the reduced activity of sulfate reducing prokaryotes at lower temperatures, and the sediment gradually shifted towards a more oxidized state. H_2S detected even in within the oxic sediment and in the rooted area in February 2018 could be attributed to the sediment heterogeneity and the presence of reducing micro-niches where anaerobic metabolism could occur regardless of surrounding redox conditions (Jørgensen, 1977; Frederiksen and Glud, 2006). Moreover, it has been found that at temperatures below 15°C, organic sulfur is more important than sulfate as a sulfide source. This was explained by a higher temperature coefficient required for sulfate reduction than for other heterotrophic processes (Jørgensen, 1977).

https://doi.org/10.5194/bg-2019-484
Preprint. Discussion started: 21 January 2020
© Author(s) 2020. CC BY 4.0 License.

In April 2018, the sediment was enriched with fresh organic matter derived from increased autotrophic biomass in bottom waters. In addition to the induction of the bloom, strong sediment resuspension, most likely by aeration, stimulated the intense oxidation of H_2S that started to produce in the rooted zone (up to 180 μM, Fig. 7), due to increased activity of sulfate reducing prokaryotes possibly triggered by the increase in temperature. An increase in S^0 concentration that reached its maximum in the same layer suggests a simultaneous oxidation of the produced H_2S. The sulfide oxidation probably caused oxygen depletion in the rooted zone and anoxic zone extension up to the sediment subsurface. In May 2018, the excess of organic matter accumulated in April 2018 was degraded. The concentrations of S^0, detected only in the suboxic layer, considerably decreased possibly by disproportionation or respiration by members of the sulfate reducing bacteria. S^0-disproportionating *Desulfobulbaceae* and S^0-respiring *Desulfuromonadales* are frequently detected in anoxic coastal sediments (Pjevac et al., 2014).

From June to August 2018, the decomposition of organic matter, encompassing the entire sediment core, was intensified and accompanied by a large increase in H_2S concentrations (up to 1200 μM). The degradation process involved rhizomes and roots, as suggested by the apparent loss of belowground biomass. Such loss typically occurs in the first stage of plant decay, the leaching phase (Trevathan-Tackett et al., 2017). Readily available, soluble carbohydrates that largely contribute to the leachate mass (Vichkovitten and Holmer, 2004) most probably supported the increase in prokaryotic abundance observed in June and July 2018. However, the significant decrease in prokaryotic abundance that coincided with a maximum degradation of organic matter and H_2S production in August 2018 might indicate that remaining compounds were not degradable by the sulfate reduction pathway (Arndt et al., 2013) and needed the presence of prokaryotes specialized in the anaerobic degradation of refractory compounds, including cellulose and lignin.

During September and October 2018, H_2S concentrations drastically decreased, and the sediment was gradually enriched in fresh organic matter. Due to the combined effect of freshened oxygenated water inflow and resuspension which gradually deepened the oxic layer, re-oxidation of H_2S increased. Biogeochemical studies suggest that most sulfides (80 – 90 %) are eventually re-oxidized, 10 – 20 % are ultimately buried as complexes with iron (i.e. FeS, FeS_2) or with organic matter after sulfurization (Jørgensen, 1977; 1982). H_2S scavenging with iron and formation of iron sulfides might be more important in Saline Bay, since terrestrial waters are washing out *terra rossa*, rich in Fe-oxides and oxyhydroxides (Durn,

https://doi.org/10.5194/bg-2019-484
Preprint. Discussion started: 21 January 2020
© Author(s) 2020. CC BY 4.0 License.

2003). For this reason, sediment cores were most likely always black with sulfuric odor, irrespective of H_2S concentrations or presence of vegetation.

5 Conclusions

During the regular growth, from July 2017 to March 2018, *C. nodosa* successfully adapted to the changes of environmental conditions and prevented H_2S accumulation by its re-oxidation, supplying the sediment with O_2 from the water column and/or leaf photosynthesis. Our results suggest that the *C. nodosa* die-off was most likely triggered in April 2018 by a reduction of light availability, which severely reduced leaf photosynthesis and the oxidation capability of belowground tissue. Simultaneously, in the sediment, depletion of oxygen due to intense oxidation of H_2S occurred, thus creating anoxic conditions in most of the rooted areas. This synergistic negative effect on the plant performance exposed *C. nodosa* to H_2S intrusion. During the degradation of dying above- and belowground tissues, which culminated in August 2018, high concentrations of H_2S were produced and accumulated all over the sediment cores, including bottom waters. An improvement in the oxygen supply in September 2018 led to the re-establishment of H_2S oxidation and recovery of the belowground tissue.

Even if the sediment conditions improved by the end of the summer 2018, *C. nodosa* has not been able to recolonize its previously occupied areas in the rest of 2018 and during 2019. This finding combined with a visible alteration of the water column and sediment is suggesting a considerable habitat loss. Further research is needed to examine the fate of Saline Bay meadows remains and an eventual recolonization of the area.

Author contribution: Conceptualization: MN, MK and GJH; Investigation: MK, PP, MM, II, LJI, IF and MN; Formal analysis and Writing - original draft: MN; Writing – review & editing: MK, GJH, PP, LJI, II, IF and MM.

Competing interests: The authors declare that they have no conflict of interest.

Acknowledgements. The financial support was provided by the Croatian Science Foundation to MN (project IP-2016-06-7118, MICRO-SEAGRASS). We sincerely thank J. Jakovčević and M. Buterer for nutrient and chlorophyll *a* determination, and A. Budiša and I. Haberle for occasional help during separation and biometry of plant material.

References

Agostini, S., Pergent, G., and Marchand, B.: Growth and primary production of *Cymodocea nodosa* in a coastal lagoon. Aquat. Bot., 76, 185-193, 2003.

Alcoverro, T., Manzanera, M., and Romero J.: Annual metabolic carbon balance of the seagrass *Posidonia oceanica*: the importance of carbohydrate reserves. Mar. Ecol. Prog. Ser., 211, 105-116, 2001.

Arndt, S., Jørgensen, B.B., LaRowe, D.E., Middelburg, J.J., Pancost, R.D., and Regnier, P.: Quantifying the degradation of organic matter in marine sediments: A review and synthesis. Earth-Science Rev., 123, 53-86, 2013.

Beca-Carretero, P., Guihéneuf, F., Marín-Guirao, L., Bernardeau-Esteller, J., García-Muñoz, R., Stengel, D.B., and Ruiz, J.M. Effects of an experimental heat wave on fatty acid composition in two Mediterranean seagrass species. Mar. Pollut. Bull., 134, 27-37, 2018.

Beca-Carretero, P., Guihéneuf, F., Winters, G., and Stengel, D.B.: Depth-induced adjustment of fatty acid and pigment composition suggests high biochemical plasticity in the tropical seagrass *Halophila stipulacea*. Mar. Ecol. Prog. Ser., 608, 105-117, 2019.

Borum, J., Pedersen, O., Greve, T.M. Frankovich, T.A., Zieman, J.C., Fourqurean, J.W., and Madden, C.J.: The potential role of plant oxygen and sulphide dynamics in die-off events of the tropical seagrass, *Thalassia testudinum*. J. Ecol., 93, 148-158, 2005.

Bourbonniere, R.A., and Meyers, P.A.: Sedimentary geolipid records of historical changes in the watersheds and productivities of Lakes Ontario and Erie. Limnol. Oceanogr., 41, 352-359, 1996.

Brodersen, K.E., Lichtenberg, M., Paz, L-C., and Kühl, M.: Epiphyte-cover on seagrass (*Zostera marina* L.) leaves impedes plant performance and radial O_2 loss from the bellow-ground tissue. Front. Mar. Sci., 2, 58 doi: 10.3389/fmars.201500058, 2015.

Cancemi, G., Buia, M.C., and Mazzella, L.: Structure and growth dynamics of *Cymodocea nodosa* meadows. Sci. Mar., 66: 365-373, 2002.

Canfield, D.E., Jørgensen, B.B., Fossing, H., Glud, R., Gundersen, J., Ramsing, N.B., Thamdrup, B., Hansen, J.W., Nielsen, L.P., and Hall, P.O.J.: Pathways of organic carbon oxidation in three continental margin sediments. Mar. Geol., 113, 27-40, 1993.

Capone, D.G., and Kiene, R.P.: Comparison of microbial dynamics in marine and freshwater sediments: Contrasts in anaerobic carbon catabolism. Limnol. Oceanogr., 33, 725-749, 1988.

Carlson, P.R., Yarbro, L.A., and Barber, T.R.: Relationship of sediment sulfide to mortality of *Thalassia testudinum*, Florida Bay. Bull. Mar. Sci., 54, 733-746, 1994.

Cline, J.D.: Spectrophotometric determination of hydrogen sulfide in natural waters. Limnol. Oceanogr., 14, 454-458, 1969.

Collier, C.J., Lavery, P.S., Masini, R.J., and Ralph, P.J.: Shade-induced response and recovery of the seagrass *Posidonia sinuosa*. J. Exp. Mar. Biol. Ecol., 370, 89-103, 2009.

Collier, J.C., Waycott, M., and Giraldo Ospina, A.: Responses of four Indo-West Pacific seagrass species to shading. Mar. Pollut. Bull., 65, 342-354, 2012.

Costa, M.M., Barrote, I., Silva, J., Olivé, I., Alexandre, A., Albano, S., and Santos, R.: Epiphytes modulate *Posidonia oceanica* photosynthetic production, energetic balance, antioxidant mechanisms, and oxidative damage. Front. Mar. Sci. 2:111, 2015.

Cranwell, P.A., Eglinton, G., and Robinson, N.: Lipids of aquatic organisms as potential contributors to lacustrine sediments. Org. Geochem., 11, 513-527, 1987.

Cúcio, C., Engelen, A.H., Costa, R., and Muyzer, G.: Rhizosphere Microbiomes of European Seagrasses Are Selected by the Plant, But Are Not Species Specific. Front. Microbiol., 7, 440. doi: 10.3389/fmicb.2016.00440, 2012.

Duarte, C.M., Middelburg, J., and Caraco, N.: Major role of marine vegetation on the oceanic carbon cycle. Biogeosciences, 2, 1-8, 2005.

Durn, G.: *Terra Rossa* in the Mediterranean Region: Parent Materials, Composition and Origin. Geologia Croatica, 56, 83-100, 2003.

Epstein, S.S., and Rossel J.: Enumeration of sandy sediment bacteria: search for optimal protocol. Mar. Ecol. Prog. Ser., 117, 289-298, 1995.

Fahimipour, A.K., Kardish, M.R., Lang, J.M., Green, J.L., Eisen, J.A., and Stachowicz, J.J.: Global-Scale Structure of the Eelgrass Microbiome. Appl. Environ. Microbiol., 83, e03391-16, 2017.

Folk, R.L.: The distinction between grain size and mineral composition in sedimentary-rock nomenclature. J. Geol., 62, 344-359, 1954.

Frederiksen, M.S., Holmer, M., Borum, J., and Kennedy, H.: Temporal and spatial variation of sulfide invasion in eelgrass (*Zostera marina*) as reflected by its sulfur isotopic composition. Limnol. Oceanogr., 51, 2308-2318, 2006.

Frederiksen, M.S., Holmer, M., Pérez, M., Invers, O., Ruiz, J.M., and Knudsen, B.: Effect of increased sediment sulfide concentrations on the composition of stable sulfur isotopes ($\delta^{34}S$) and sulfur accumulation in the seagrasses *Zostera marina* and *Posidonia oceanica*. J. Exp. Mar. Biol. Ecol., 358, 98-109, 2008.

Frederiksen, M.S., and Glud, R.N.: Oxygen dynamics in the rhizosphere of *Zostera marina*: A two-dimensional planar optode study. Limnol. Oceanogr., 51, 1072-1083, 2006.

https://doi.org/10.5194/bg-2019-484
Preprint. Discussion started: 21 January 2020
© Author(s) 2020. CC BY 4.0 License.

Gacia, E., and Duarte, C.M.: Sediment Retention by a Mediterranean *Posidonia oceanica* Meadow: The Balance between Deposition and Resuspension. Estuar. Coast. Shelf. Sci., 52, 505–514, 2001.

Gangi, A.F.: Permeability of unconsolidated sands and porous rocks. J. Geophys. Res. –Solid, 90, 3099-3104, 1985.

Greve, T.M., Borum, J., and Pedersen, O.: Meristematic oxygen variability in eelgrass (*Zostera marina*). Limnol. Oceanogr., 48, 210-216, 2003.

Halun, Z., Terrados, J., Borum, J., Kamp-Nielsen, J., Duarte, C.M., and Fortes, M.D.: Experimental evaluation of the effects of siltation-derived changes in sediment conditions on the Philippine seagrass *Cymodocea rotundata*. J. Exp. Mar. Biol. Ecol., 279, 73-87, 2002.

Harris, R.V., and James, A.T.: Linoleic and α-linolenic acid biosynthesis in plant leaves and a green alga. Biochim. Biophys. Acta, 106, 456-464, 1965.

Hasler-Sheetal, H., and Holmer, M.: Sulfide intrusion and detoxification in the seagrass *Zostera marina*. Plos One 10(6): e0129136, 2015.

Hendriks, I.E., Sintes, T., Bouma, T.J., and Duarte, C.M.: Experimental assessment and modeling evaluation of the effects of the seagrass *Posidonia oceanica* on flow and particle trapping. Mar. Ecol. Prog. Ser., 356, 163-173, 2008.

Holm-Hansen, O., Lorenzen, C. J., Holmes, R. W., and Strickland, J. D. H.: Fluorometric determination of chlorophyll. J. Conseil., 301, 3-15, 1965.

Holmer, M., Duarte, C.M., Boschker, H.T.S., and Barrón, C.: Carbon cycling and bacterial carbon sources in pristine and impacted Mediterranean seagrass sediments. Aquat. Microb. Ecol., 36, 227-237, 2004.

Holmer, M., and Hasler-Sheetal, H.: Sulfide intrusion in seagrasses assessed by stable isotopes- a synthesis of current results. Front. Mar. Sci., doi: 10.3389/fmars.2014.00064, 2014.

Holmer, M., and Nielsen, S.L.: Sediment sulfur dynamics related to biomass-density pattern in *Zostera marina* (eelgrass) beds. Mar. Ecol. Prog. Ser., 146, 163-171, 1997.

Holmer, M., Frederiksen, M.S., and Møllegaard, H.: Sulfur accumulation in eelgrass (*Zostera marina*) and effect of sulfur on eelgrass growth. Aquat. Bot., 81, 367-379, 2005.

Holmer, M., Pedersen, O., and Ikejima, K.: Sulfur cycling and sulfide intrusion in mixed Southeast Asian tropical seagrass meadows. Bot. Mar., 49, 91-102, 2006.

Ivančić, I., Paliaga, P., Pfannkuchen, M., Đakovac, T., Najdek, M., Steiner, P., Korlević, M., Markovski, M., Baričević, A., Smodlaka Tanković, M., and Herndl, G.J.: Seasonal

https://doi.org/10.5194/bg-2019-484
Preprint. Discussion started: 21 January 2020
© Author(s) 2020. CC BY 4.0 License.

variations in extracellular enzymatic activity in marine snow-associated microbial communities and their impact on the surrounding water. FEMS Microbiol. Ecol., 94, fyi198, 2018.

Iveša, Lj., Blažina, M., and Najdek, M.: Seasonal variations in fatty acid composition of *Caulerpa taxifolia* (M. Vahl.) C. Ag. in the northern Adriatic Sea (Malinska, Croatia). Bot. Mar., 47, 209-214, 2004.

Jensen, S.I., Kühl, M., and Priemé, A.: Different Bacterial Communities Associated with the Roots and Bulk Sediment of the Seagrass *Zostera marina*. FEMS Microbiol. Ecol., 62, 108-117, 2007.

Jørgensen, B.B.: The sulfur cycle of a coastal marine sediment (Limfjorden, Denmark). Limnol. Oceanogr., 22, 814-832, 1977.

Jørgensen, B.B.: Mineralization of organic matter in the sea bed - the role of sulphate reduction. Nature, 296, 643-645, 1982.

Koch, M.S., and Erskine, J.M.: Sulfide as a Phytotoxin to the Tropical Seagrass *Thalassia testudinum*: Interactions with Light, Salinity and Temperature. J. Exp. Mar. Biol. Ecol., 266, 81-95, 2001.

Krause-Jensen, D., Carstensen, J., Nielsen, S.L., Dalsgaard, T., Christensen, P.B., Fossing, H., and Rasmussen, M.B.: Sea bottom characteristics affect depth limits of eelgrass *Zostera marina*. Mar. Ecol. Prog. Ser., 425, 91-102, 2011.

Lee, K-S., and Dunton, K.H.: Effects of *in situ* light reduction on the maintenance, growth and partitioning of carbon resources in *Thalassia testidinum* at Banks ex König. J. Exp. Mar. Biol. Ecol., 210, 53-73, 1997.

Lee, K-S., and Dunton, K.H.: Diurnal changes in pore water sulfide concentrations in the seagrass *Thalassia testudinum* beds: the effects of seagrasses on sulfide dynamics. J. Exp. Mar. Biol. Ecol., 255, 201-214, 2000.

Lee, K-S., Park, S.R., and Kim, Y.K.: Effects of irradiance, temperature, and nutrients on growth dynamics of seagrasses: A review. J. Exp. Mar. Biol. Ecol., 350, 144-175, 2007.

Marbà, N., Cebrián, J., Enríquez, S., and Duarte, C.M.: Growth patterns of Western Mediterranean seagrasses: species specific responses to seasonal forcing. Mar. Ecol. Prog. Ser., 133, 203-215, 1996.

Marbà, N., and Duarte, C.M.: Growth and sediment space occupation by seagrass *Cymodocea nodosa* roots. Mar. Ecol. Prog. Ser., 224, 291-298, 2001.

https://doi.org/10.5194/bg-2019-484
Preprint. Discussion started: 21 January 2020
© Author(s) 2020. CC BY 4.0 License.

Mascaró, O., Valdemarsen, T., Holmer, M., Pérez, M., and Romero, J.: Experimental manipulation of sediment organic content and water column aeration reduces *Zostera marina* (eelgrass) growth and survival. J. Exp. Mar. Biol. Ecol., 373, 26-34, 2009.

Micromeritics: SediGraph 5100 particle size analysis system operator' manual. Micromeritics Instrument Corporation, Norcross, 2002.

Moeslund, L., Thamdrup, B., and Jørgensen, B.B.: Sulfur and iron cycling in a coastal sediment—radiotracer studies and seasonal dynamics. Biogeochemistry, 27, 129-152, 1994.

Nicholls, P., Marshall, D.C., Cooper, C.E., and Wilson, M.T.: Sulfide inhibition of and metabolism by cytochrome c oxidase. Biochem. Soc. Transact., 41, 1312-1316, 2013.

Orth, R.J., Carruthers, T.J.B., Dennison, W.C., Duarte, C.M., Fourqurean, J.W., Heck Jr., K.L., Hughes, A.R., Kendrick, G.A., Kenworthy, E.J., Olyarnik, S., Short, F.T., Waycott, M., and Williams, S.L.: A Global Crisis for Seagrass Ecosystems. BioScience 56, 987-996, 2006.

Panutrakul, S., Monteny, F., and Baeyens, W.: Seasonal Variations in Sediment Sulfur Cycling in the Ballastplaat Mudflat, Belgium. Estuaries 24, 257-265, 2001.

Pedersen, M.F., Duarte, C.M., and Cebrián, J.: Rates of changes in organic matter and nutrient stocks during seagrass *Cymodocea nodosa* colonization and stand development. Mar. Ecol. Prog. Ser., 159, 29-36, 1997.

Pedersen, O., Borum, J., Duarte, C.M., and Fortes, M.D.: Oxygen dynamics in the rhizosphere of *Cymodocea rotundata*. Mar. Ecol. Prog. Ser., 169, 283-288, 1988.

Pedersen, O., Binzer, T., and Borum, J.: Sulphide intrusion in eelgrass (*Zostera marina* L.). Plant Cell Environ., 27, 595-602, 2004.

Peduzzi, P., and Herndl, G.J.: Decomposition and significance of seagrass litter (*Cymodocea nodosa*) for the microbial food web in coastal waters (Gulf of Trieste, Northern Adriatic Sea). Mar. Ecol. Prog. Ser., 71, 163-174, 1991.

Pérez, M., Invers, O., Ruiz Fernandez, J.M., Frederiksen, M., and Holmer, M.: Physiological responses of the seagrass *Posidonia oceanica* to elevated organic matter content in sediments: An experimental assessment. J. Exp. Mar. Biol. Ecol., 344,149-160, 2007.

Pirini, M., Manuzzi, M.P., Pagliarani, A., Trombetti, F., Borgatti, A.R., and Ventrella, V.: Changes in fatty acid composition of *Mytilus galloprovincialis* (Lmk) fed on microalgal and wheat germ diets. Comp. Biochem. Physiol. B, 147, 616-626, 2007.

Pjevac, P., Kamyshny Jr., A., Dyksma, S., and Mussmann, M.: Microbial consumption of zero-valence sulfur in marine benthic habitats. Environ. Microbiol., 16, 3416-3430, 2014.

Porter, K.G., and Feig, Y.S.: The use of DAPI for identification and counting aquatic microflora. Limnol. Oceanogr., 25, 943-984, 1980.

Quigg, A., Kevekordes, K., Raven, J., and Beardall, J.: Limitations on microalgal growth at very low photon fluency rates: the role of energy slippage. Photosynth. Res., 88, 299-310, 2006.

Rogowska, J., Sychowska, J., Cieszynska-Semenowicz, M., and Wolska, L.: Elemental sulfur in sediments: analytical problems. Environ. Sci. Pollut. Res., 23, 24871-24879, 2016.

Sand-Jensen, K., Pedersen, O., Binzer, T., and Borum, J.: Contrasting Oxygen Dynamics in the Freshwater Isoetid *Lobelia dortmanna* and the Marine Seagrass *Zostera marina*. Ann. Bot., 96, 613-623, 2005.

Schmid, M., Guihéneuf, F., and Stengel, D.B.: Fatty acid contents and profiles of 16 macroalgae collected from the Irish Coast at two seasons. J. Appl. Phycol., 26, 451-463, 2014.

Sousa, A.I., Calado, R., Cleary, D.F.R., Nunes, C., Coimbra, M.A., Serôdio, J., and Lillebø, A.I.: Effect of spatio-temporal shifts in salinity combined with other environmental variables on the ecological processes provided by *Zostera noltii* meadows. Sci. Rep., 7, 1336, 2017.

Strickland, J.D.H., and Parsons, T.R.: A practical handbook of seawater analysis. Bull. Fish. Res. Board. Can., 167,1-310, 1972.

Terrados, J., and Lopez-Jimenez, J.A.: Fatty acid composition and chilling resistance in the green alga *Caulerpa prolifera* (Forrskal) Lamouroux (Chlorophyta, Caulerpales).Biochem. Molecul. Biol. Internatl., 39, 863-869, 1996.

Terrados, J., Duarte, C.M., Fortes, M.D., Borum, J., Agawin, N.S.R., Bach, S., Thampanya, U., Kamp-Nielsen, L., Kenworthy, W.J., Geertz-Hansen, O., and Vermaat, J.: Changes in Community Structure and Biomass of Seagrass Communities along Gradients of Siltation in SE Asia. Estuar. Coast. Shelf Sci., 46, 757-768, 1998.

Terrados, J., and Ros, J.D.: Growth and primary production of *Cymodocea nodosa* (Ucria) Ascherson in a Mediterranean coastal lagoon: the Mar Menor (SE Spain). Aquat. Bot., 43, 63-74, 1992.

Trevathan-Tackett, S.M., Seymour, J.R., Nielsen, D.A., Macreadie, P.I., Jeffries, T.C., Sanderman, J., Baldock, J., Howes, J.M., Steven, A.D.L., and Ralph, P.J.: Sediment anoxia limits microbial-driven seagrass carbon remineralization under warming conditions. FEMS Microbiol. Ecol., 93,fix033, 2017.

https://doi.org/10.5194/bg-2019-484
Preprint. Discussion started: 21 January 2020
© Author(s) 2020. CC BY 4.0 License.

Troelsen, H., and Jørgensen, B.B.: Seasonal dynamics of elemental sulfur in two coastal sediments. Estuar. Coast. Shelf Sci., 15, 255-266, 1982.

Ugarelli, K., Chakrabarti, S., Laas, P., and Stingl, U.: The seagrass holobiont and its microbiome. Microorganisms 5, 81, 2017.

Upchurch, R.G.: Fatty acid unsaturation, mobilization, and regulation in the response of plants to stress. Biotechnol. Lett., 30, 967-977, 2008.

Vaquer-Sunyer, R., and Duarte, C.M.: Thresholds of hypoxia for marine biodiversity. PNAS, 105, 15452-15457, 2008.

Vaquer-Sunyer, R., and Duarte, C.M.: Sulfide exposure accelerates hypoxia-driven mortality. Limnol. Oceanogr., 55, 1075-1082, 2010.

Viso, A.C., Pesando, D., Bernard, P., and Marty, J.C.: Lipid components of the Mediterranean seagrass *Posidonia oceanica*. Mar. Pollut. Bull., 34, 381-387, 1993.

Vichkovitten, T., and Holmer, M.: Contribution of plant carbohydrates to sedimentary carbon mineralization. Org. Geochem., 35,1053-1066, 2004.

Wacker, A., Piepho, M., Harwood, J.L., Guschina, I.A., and Arts, M.T.: Light-induced changes in fatty acid profiles of specific lipid classes in several freshwater phytoplankton species. Front. Plant Sci., 7, 264, 2016.

Wasmund, K., Mußmann, M., and Loyet, A.: The life sulfuric: microbial ecology of sulfur cycling in marine sediments. Environ. Microbiol. Rep., 9, 323-344, 2017.

Widdows, J., Pope, N.D., Brinsley, M.D., Asmus, H., and Asmus, R.M.: Effects of seagrass beds (*Zostera noltii* and *Z. marina*) on near-bed hydrodynamics and sediment resuspension. Mar. Ecol. Prog. Ser., 358, 125-136, 2008.

Zavodnik, N., Travizi, A., and De Rosa, S.: Seasonal variations in the rate of photosynthetic activity and chemical composition of the seagrass *Cymodocea nodosa* (Ucr.) Asch. Sci. Mar., 62, 301-309, 1998.

Zopfi, J., Ferdelman, T.G., and Fossing, H.: Distribution and fate of sulfur intermediates - sulfite, tetrathionate, thiosulfate, and elemental sulfur in marine sediments. Geol. Soc. Am., 379, 2004.

https://doi.org/10.5194/bg-2019-484
Preprint. Discussion started: 21 January 2020
© Author(s) 2020. CC BY 4.0 License.

Biogeosciences
Discussions
Open Access

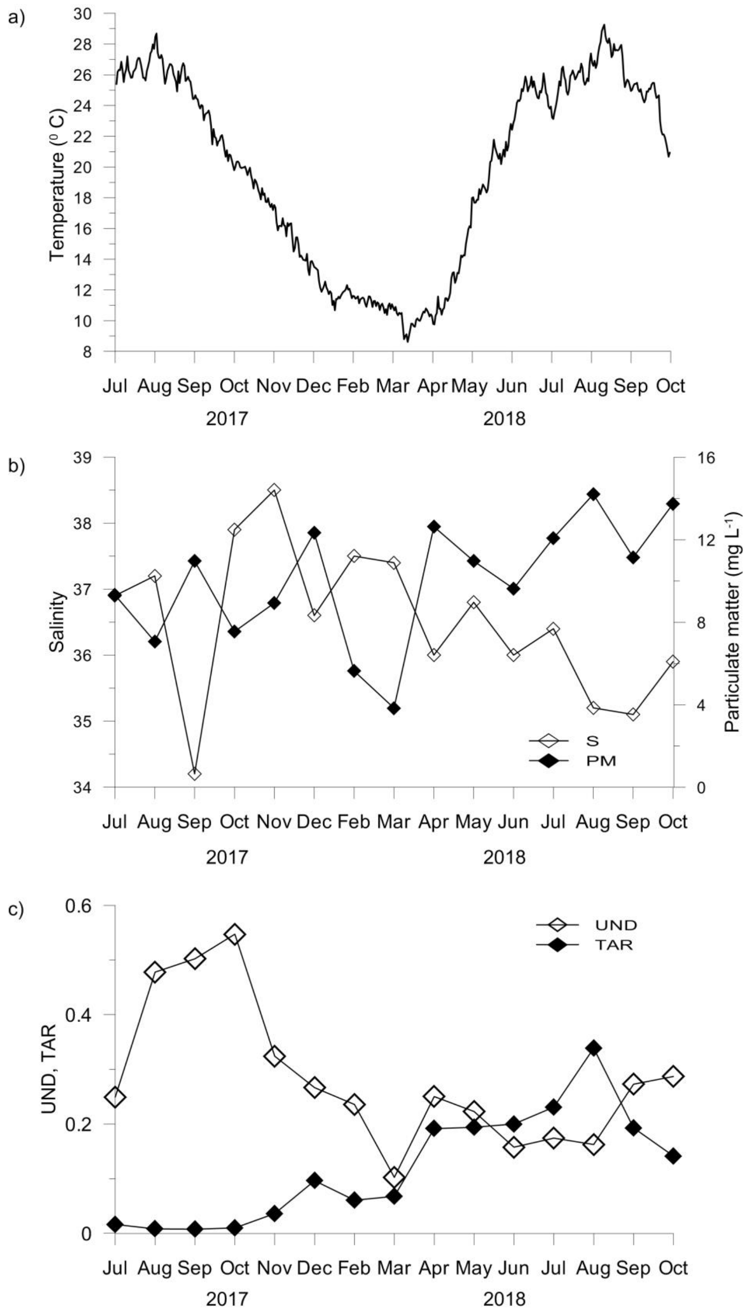

Figure 1. Temperature (a); salinity (b), particulate matter concentration (b); unsaturation degree (UND) and terrestrial to aquatic ratio (TAR) of the particulate lipid matter (c) in seawater.

https://doi.org/10.5194/bg-2019-484
Preprint. Discussion started: 21 January 2020
© Author(s) 2020. CC BY 4.0 License.

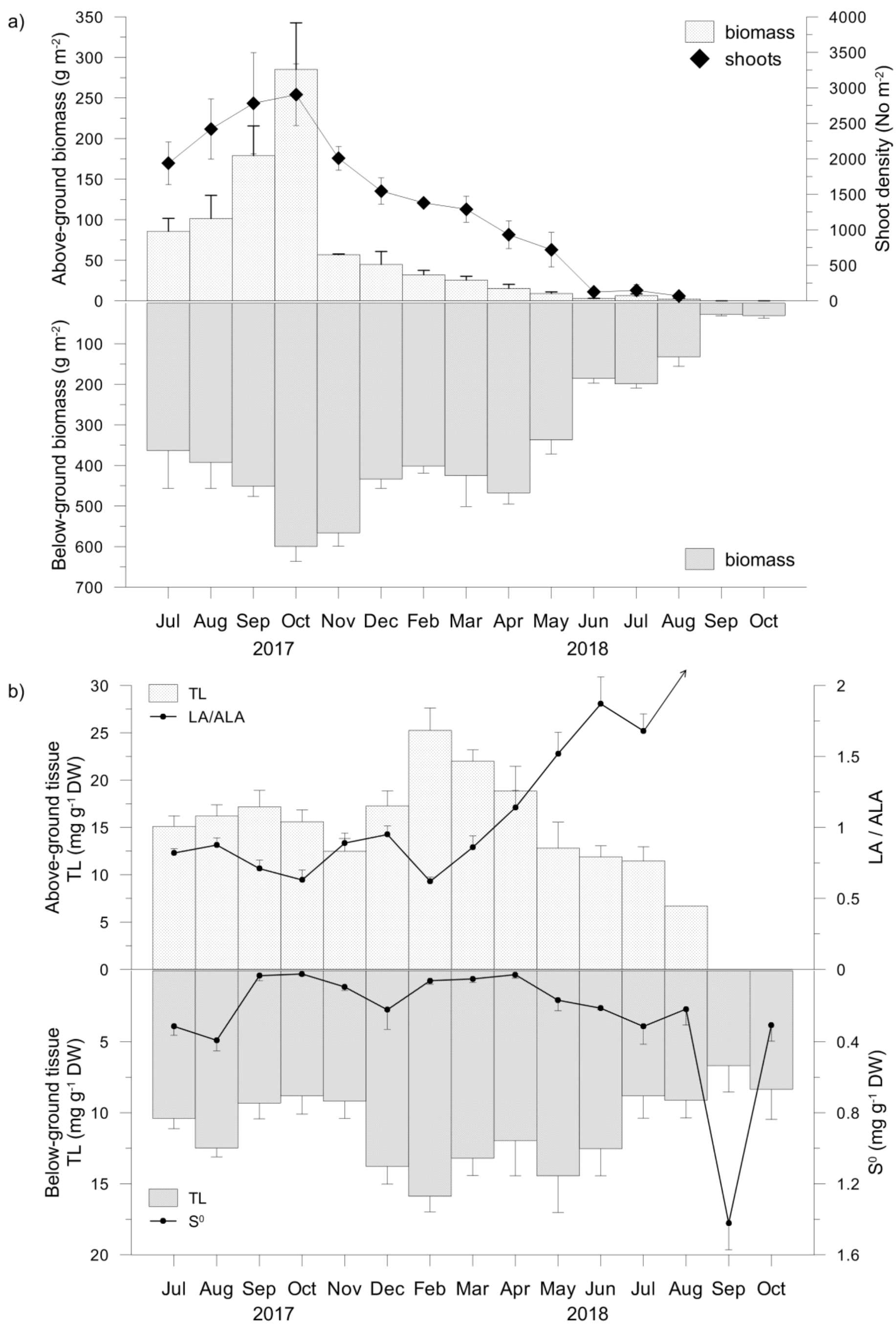

Figure 2. Above- and below-ground tissue biomasses and shoot density (a), total lipid concentrations (TL) and linoleic to α-linolenic fatty acids ratios (LA/ALA, an arrow indicates an infinite value) in above-ground tissue and TL and approximated concentrations of elemental sulfur (S^0) in below-ground tissue (b).

https://doi.org/10.5194/bg-2019-484
Preprint. Discussion started: 21 January 2020
© Author(s) 2020. CC BY 4.0 License.

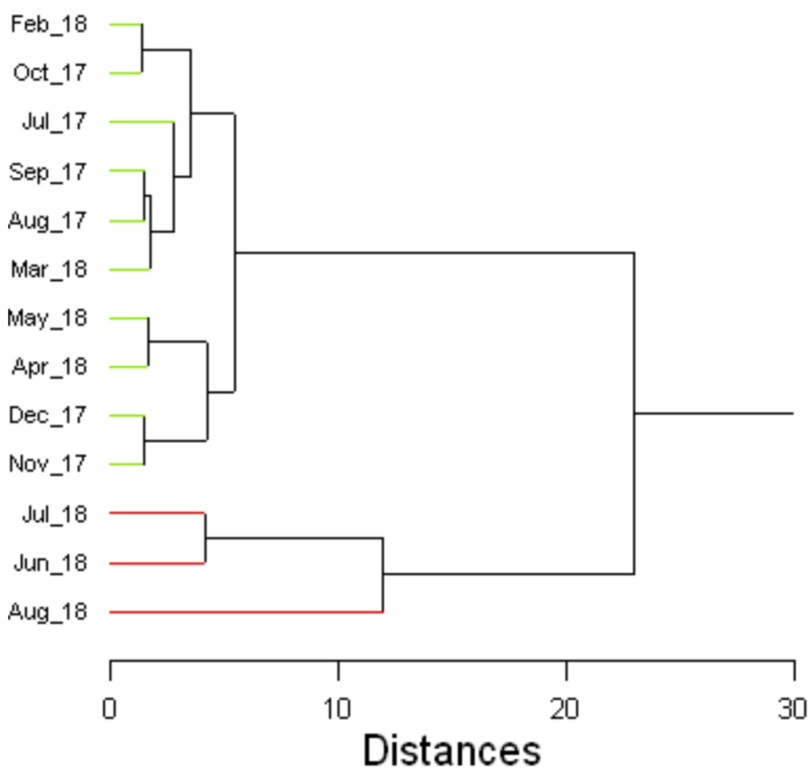

946
947 Figure 3. Cluster analysis dendrogram of fatty acid composition of *C. nodosa* leaves.
948 Summary statistics is given in Table S3.

https://doi.org/10.5194/bg-2019-484
Preprint. Discussion started: 21 January 2020
© Author(s) 2020. CC BY 4.0 License.

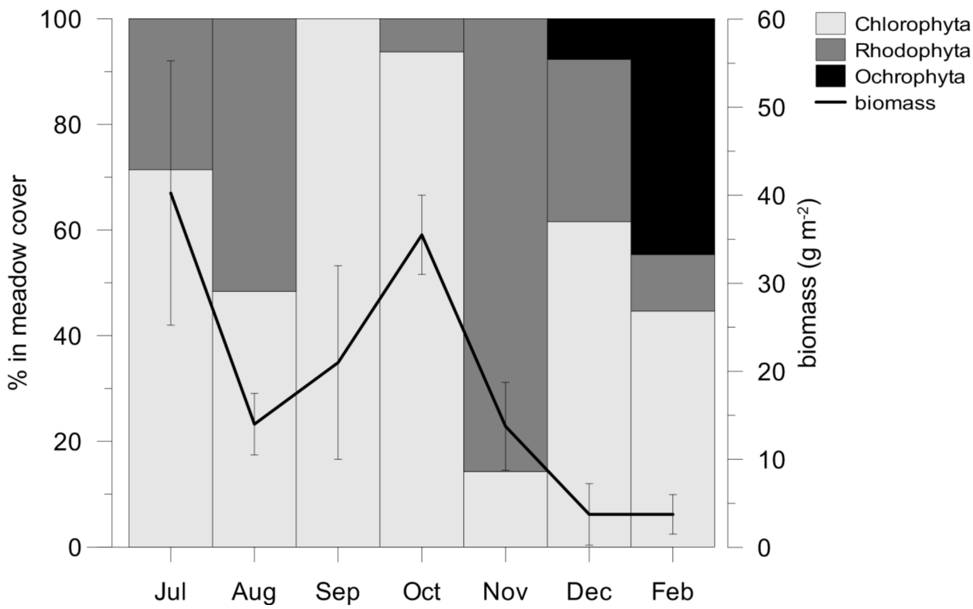

Figure 4. The contribution of macroalgal phyla in a meadow cover and total macroalgal biomass changes during their notable presence in a *C. nodosa* meadow.

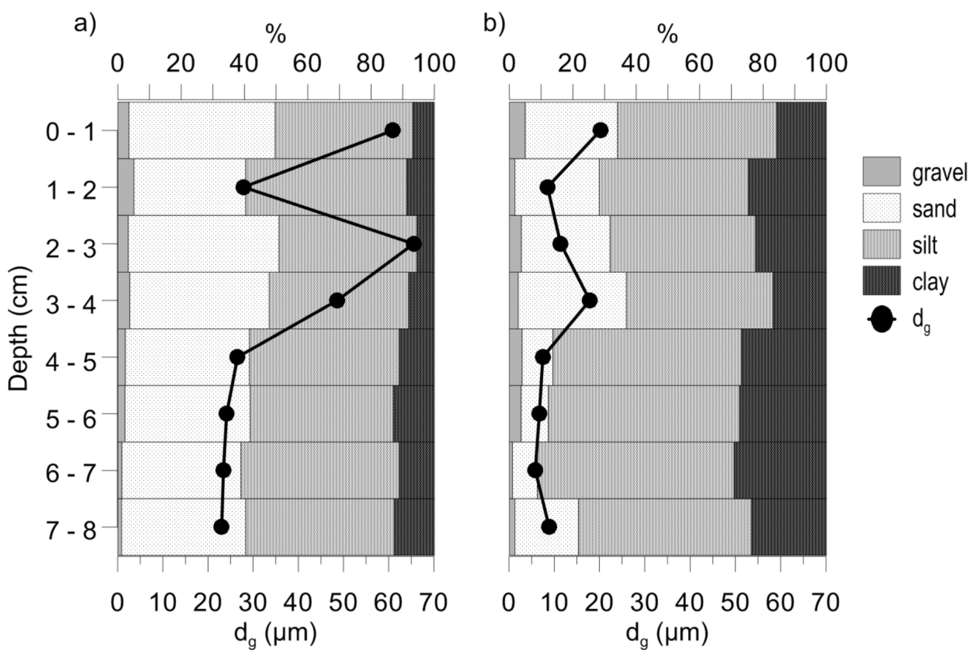

Figure 5. Granulometric composition and median grain size (d_g) of vegetated (a) and non-vegetated sediment (b).

https://doi.org/10.5194/bg-2019-484
Preprint. Discussion started: 21 January 2020
© Author(s) 2020. CC BY 4.0 License.

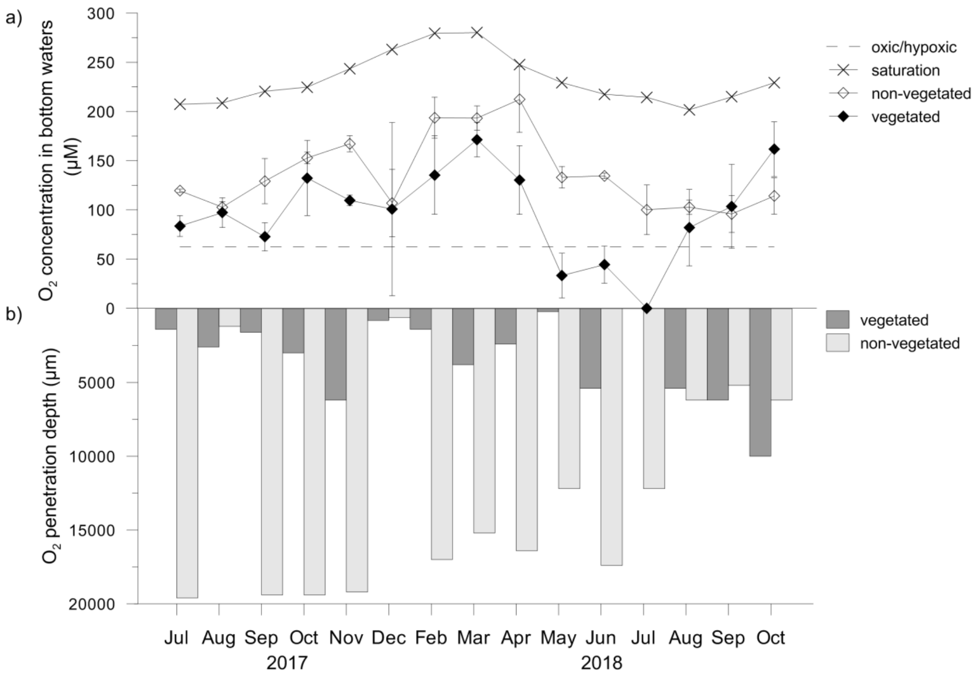

Figure 6. Oxygen concentrations (O_2) in bottom waters (a) and O_2 penetration depths (b) above and in vegetated and non-vegetated sediment, respectively. O_2 at the saturation level was calculated according to the temperature and salinity measured in seawater at the sampling dates; O_2 at the hypoxic frontier (~ 62.5 µM) was taken from Vaquer-Sanyer and Duarte (2008).

https://doi.org/10.5194/bg-2019-484
Preprint. Discussion started: 21 January 2020
© Author(s) 2020. CC BY 4.0 License.

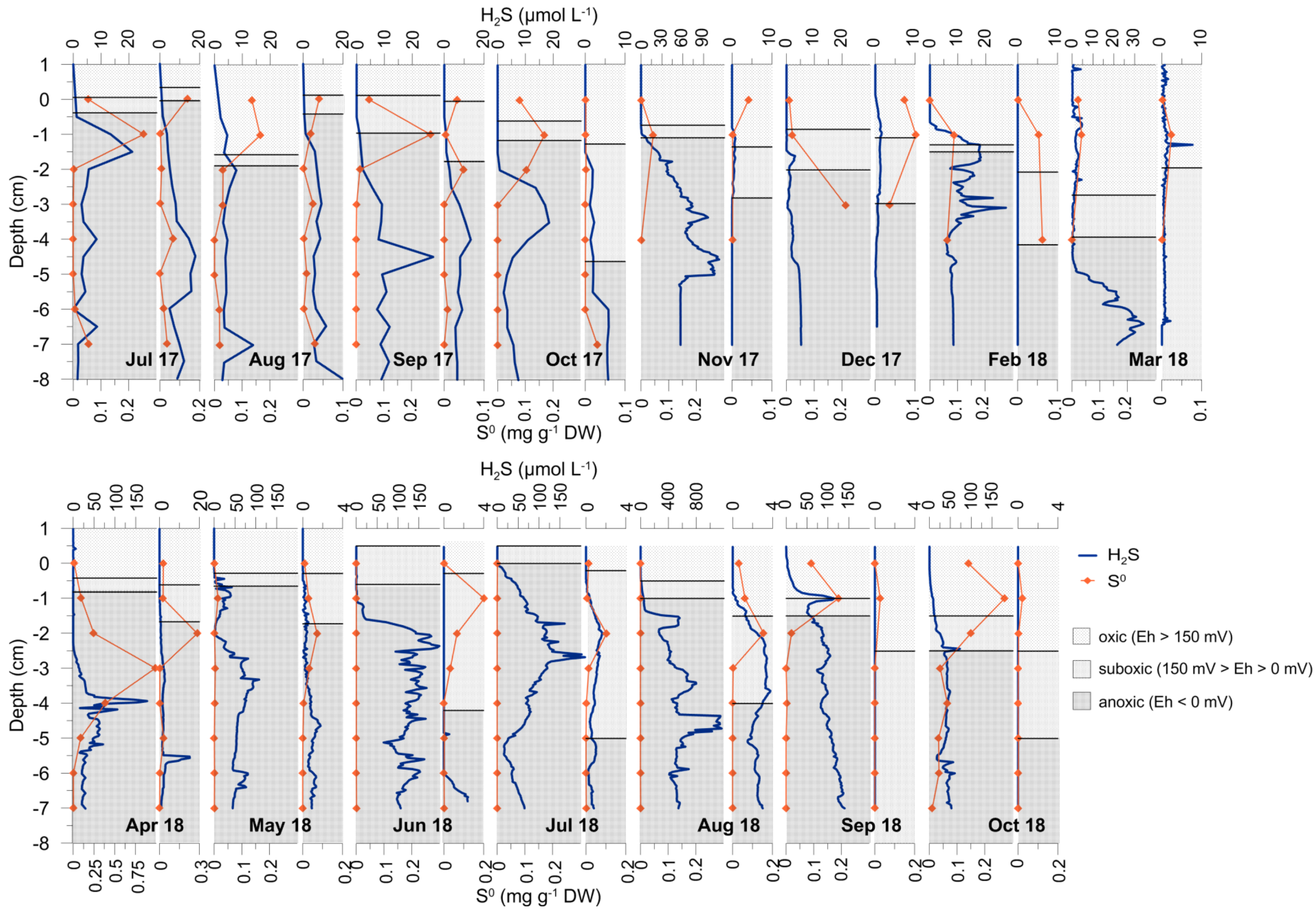

Figure 7. Depth profiles of H_2S and S^0 concentrations in vegetated and non-vegetated sediment (adjacent narrow graphs). The redox potential (Eh) in both sediments is shown as areas corresponding to oxic (Eh > 150 mV), suboxic (150 > Eh > 0 mV) and anoxic (Eh < 0 mV) conditions.

https://doi.org/10.5194/bg-2019-484
Preprint. Discussion started: 21 January 2020
© Author(s) 2020. CC BY 4.0 License.

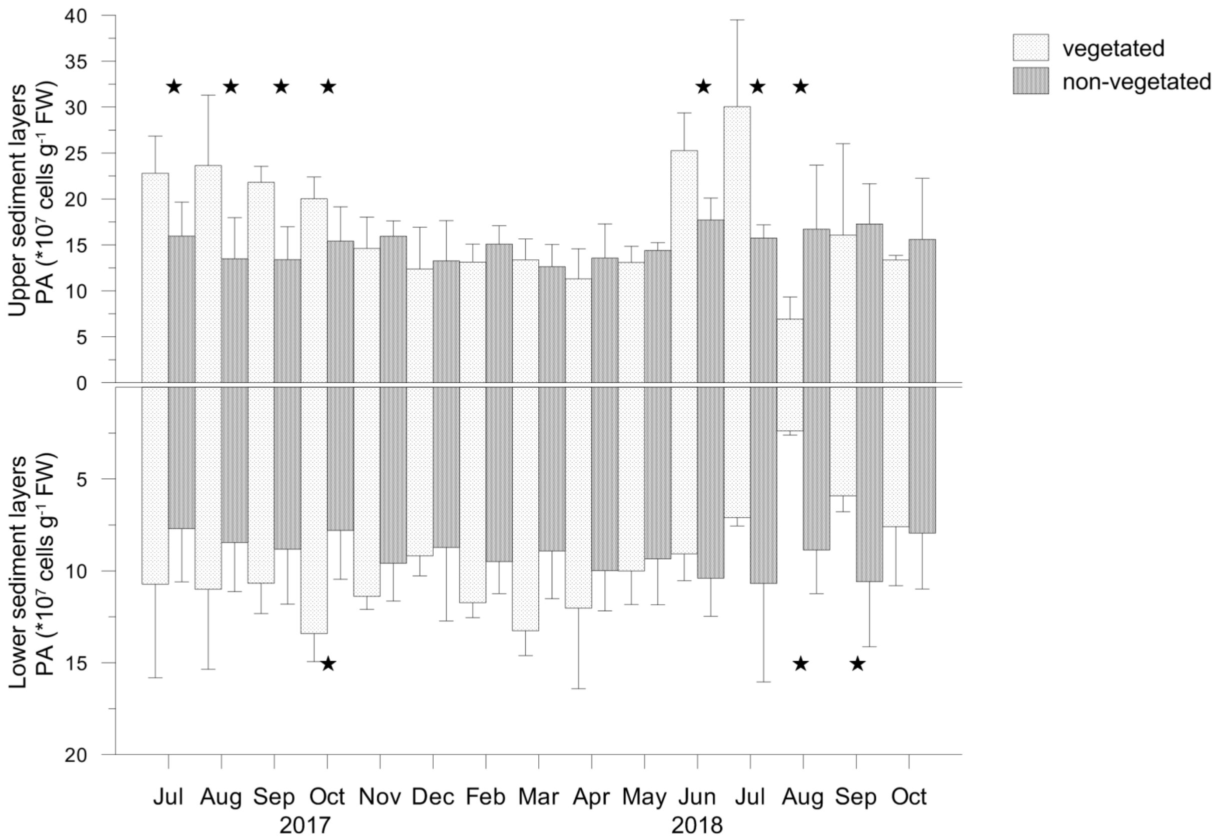

Figure 8. Prokaryotic abundance (PA) in the upper (0 - 4 cm) and lower (5 - 8 cm) layers of vegetated and non-vegetated sediments; significant differences in PA between the sediments are indicated by asterisks.

https://doi.org/10.5194/bg-2019-484
Preprint. Discussion started: 21 January 2020
© Author(s) 2020. CC BY 4.0 License.

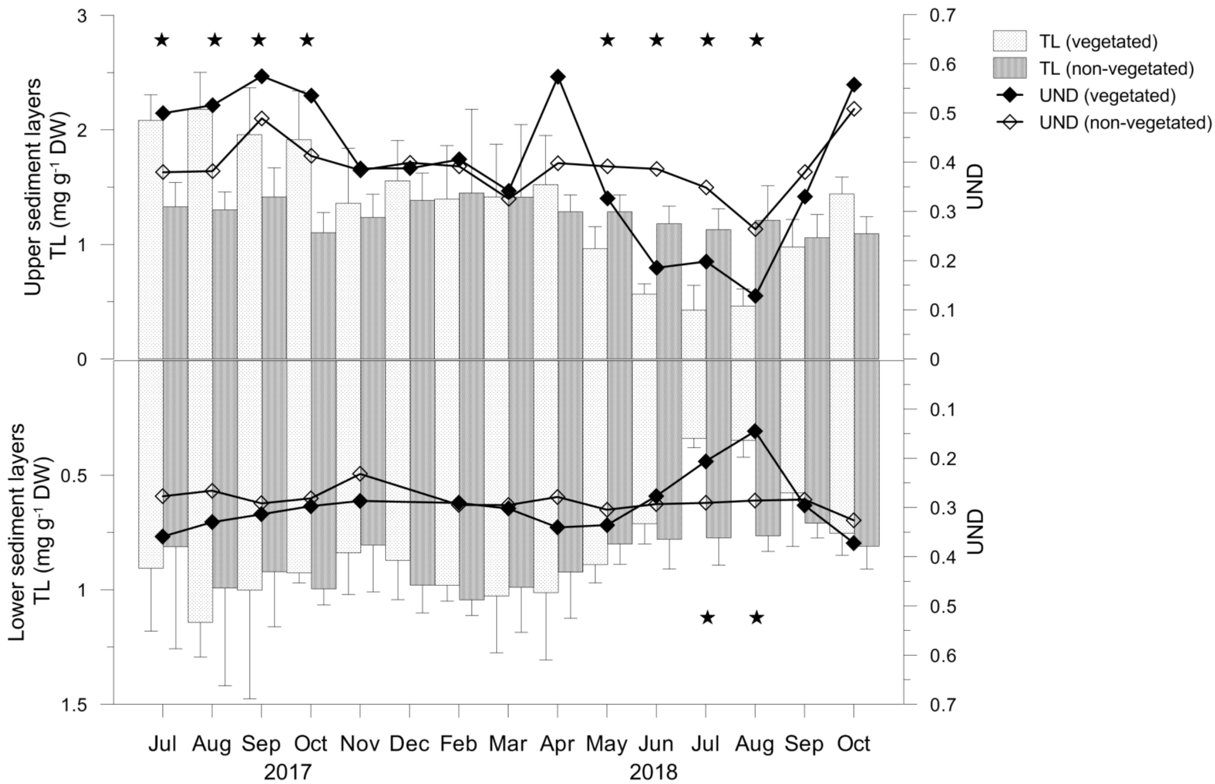

Figure 9. Total lipid concentrations (TL) and unsaturation degree (UND) in the upper (0 - 4 cm) and lower (5 - 8 cm) layers of vegetated and non-vegetated sediments. Significant differences in TL between the sediments are indicated by asterisks.

https://doi.org/10.5194/bg-2019-484
Preprint. Discussion started: 21 January 2020
© Author(s) 2020. CC BY 4.0 License.

Biogeosciences
Discussions
Open Access
EGU

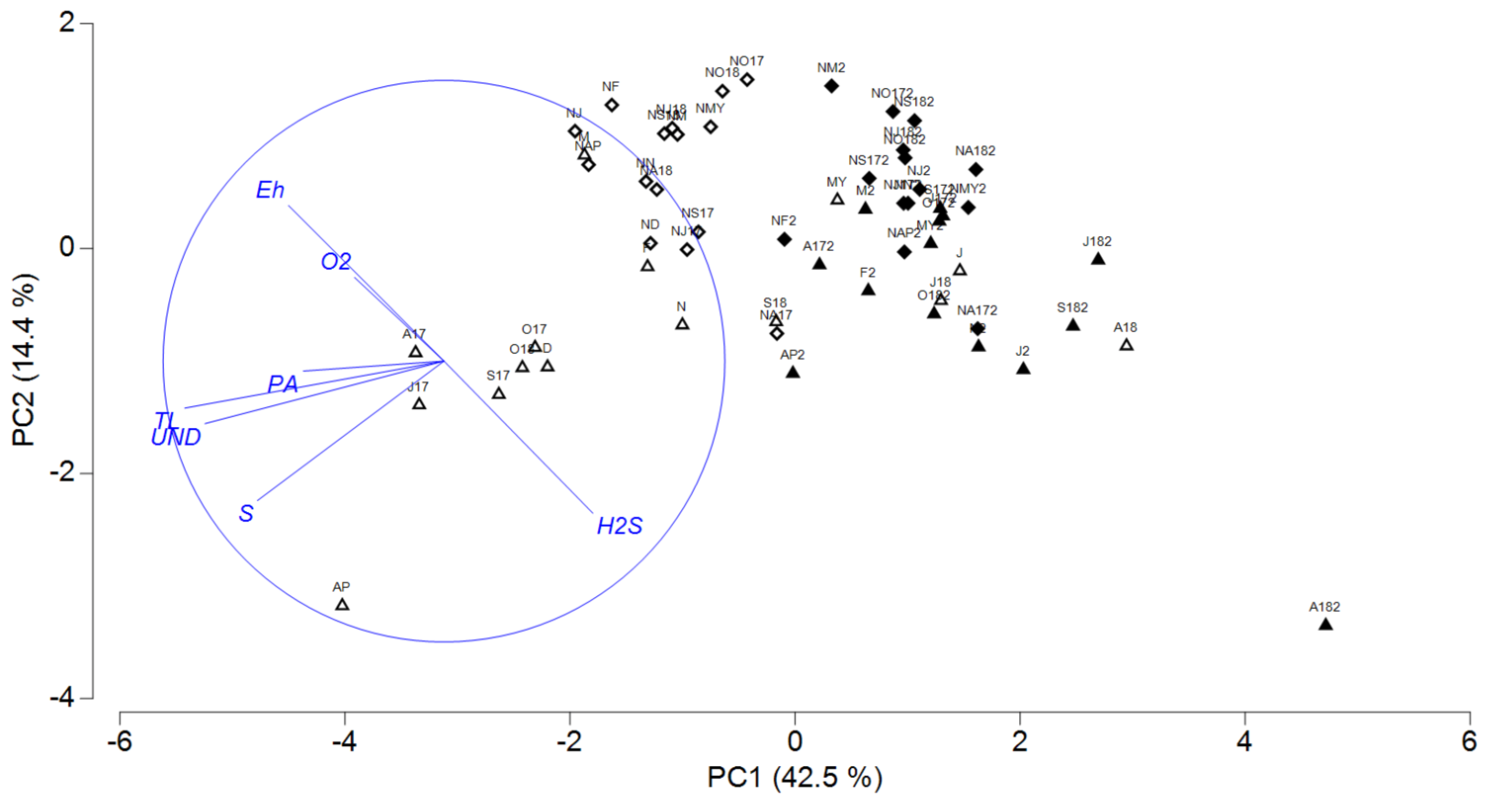

Figure 10. PCA plot of redox potential (Eh), oxygen (O_2), hydrogen sulfide (H_2S), sulfur (S), total lipids (TL) and prokaryotes (PA) concentrations and unsaturation degree (UND) in the upper (0 – 4 cm; △, ◇) and lower (5 – 7 cm; ▲, ◆) layers of vegetated and non-vegetated sediments, respectively. Projections of variables are given in circles.